New insights on asymmetric folding by means of the anisotropy of magnetic susceptibility, Variscan and Pyrenean folds (SW Pyrenees)

Belén Oliva-Urcia (1,2), Inma Gil-Peña (3), Ruth Soto (4), José María Samsó (5), Borja Antolín (2,6), Emilio L. Pueyo (4)

(1) Dept. Geología y Geoquímica. Universidad Autónoma de Madrid. belen.oliva@uam.es
(2) Dpto. Ciencias de la Tierra, Universidad de Zaragoza, Spain
(3) IGME, C/Ríos Rosas 23, 28003, Madrid, Spain
(4) IGME, Unidad de Zaragoza, C/ Manuel Lasala 44, 9º, 50006 Spain
(5) Consulting Geologist, C/ Mayor 30, 1º Jaca, Spain
(6) Dept. of Geological Sciences and Geological Engineering, Queen's University, Kingston, Ontario, Canada

ABSTRACT

The main goal of this work is to compare the magnetic fabric and field structural observations of the limbs of seven asymmetric folds in the Pyrenees to determine the differences of internal deformation as well as the folding kinematics. The magnetic fabric allows to unravel the petrofabric of these folded sedimentary rocks with scarce strain markers. Three folds developed during the Variscan Orogeny in Ordovician and Devonian rocks, and four folds developed during the Pyrenean Orogeny in Eocene rocks, were studied. Folds show a variety of structural locations, in different thrust sheets of the Southern Central Pyrenees, different cleavage development, age, geometry and lithology. Sampling follows an equivalent lithological layer in the two limbs except in one case of the selected folds. A modified tectonic magnetic fabric is found in most sites showing the magnetic lineation (k_{max}) on the tectonic foliation plane. A larger scattering of the k_{max} axes and a higher intensity of the preferred orientation of minerals (eccentricity of the AMS ellipsoid) is better observed in the overturned (short) limb of the asymmetric Variscan folds than in the normal (long) limb, while shape parameter in Alpine folds is generally larger in the overtured (short) limb respect to the normal (long) one, a good clustering of k_{min} axes is observed in all limbs.

The combination of the AMS data with the structural data helps to understand and better constrain the deformation degree in these asymmetric folds and to unravel the deformational history.

Keywords: AMS, folds, asymmetric, folding mechanism, Pyrenees

INTRODUCTION

Folds constitute common geological elements that may develop in all tectonic environments, being more abundant in fold and thrust belts. During the last decades, numerous works have dealt with folding focused on the geometry of the folded strata and the possible deformation mechanisms during folding deduced from the study of their geometry and/or internal features (e.g. *(Donath and Parker, 1964; Ghosh, 1966; Ramsay, 1967; Suppe, 1985; Jamison, 1987*). However, the internal strain that provides insight about deformation mechanisms still needs to be linked to macroscopic geometrical models that describe the kinematics of folding (*Amrouch et al., 2011* and references therein). In this sense, analysis of the petrofabric associated to strain in folded rocks can contribute to understand folding mechanism and its deformation history. However, in numerous folds, strain markers are scarce rendering useful an analysis of the anisotropy of the magnetic susceptibility (AMS). The parallelism between the fabric due to deformation and the magnetic fabric is already known from numerous publications since the early works on AMS analyses *(Graham, 1954; Stone, 1962; Graham, 1966; Kneen, 1976; Borradaile, 1988; Borradaile and Tarling, 1981; Rathore and Henry, 1982; Borradaile and Jackson, 2004)*.

This parallelism is used in a wide array of tectonic regimes, from sedimentary basins where the main extensional direction is parallel to the magnetic lineation (*Alfonsi, 1997; Mattei et al., 1997; Cifelli et al., 2005)* to compressional settings, where the magnetic lineation, parallel to the elongation direction, is at large angle to the compression (*Borradaile and Tarling, 1981; Kligfield et al., 1981; Hrouda, 1982 ;Borradaile, 1988; Aubourg et al., 1995; Lüneburg et al., 1999; Parés et al., 1999).* Recent works aiming to decipher the extensional direction in inverted basins using magnetic fabrics as strain marker, suggest that the development of a new fabric on consolidated rocks due to a late compressional event requires a strong deformation to overcome the primary extensional fabric, such as the development of tectonic foliations (*García-Lasanta et al., 2016*). The transformation of the fabric is described even in areas where no macroscopic tectonic foliation is observed but where subtle compressional features at the microscopic scale are found (*Oliva-Urcia et al., 2013*). In foreland basin sediments, the compression develops a tectonic primary fabric due to early layer parallel shortening (*Soto et al., 2009*).

A primary fabric later affected by a strong compression event and resulting in a tectonic foliation, a flexural folding, shearing (i.e., thrust related) and/or flattening, may become partially (composite fabric) (*Debacker et al., 2004*) or totally (new compressive fabric) overprinted *(Mamtani et al., 1999; Kadzialko-Hofmokl et al., 2004; Anderson and Morris, 2004; Mukherji et al., 2004; Mamtani and Sengupta, 2010).* The imprint of these different tectonic events on the fabric can be studied using AMS data. The magnetic study must be conducted together with magnetic mineral analyses, since the addition of tectonic events may affect not only the relationship between AMS and strain but also the mineralogy of the rocks *(Borradaile, 1987; Hrouda, 1987; Housen and van der Pluijm, 1990;*

Jackson, 1991; Debacker et al., 2009). For example, it has been known that different deformation events can be preserved by different magnetic carriers (e.g., *Hirt et al., 2008; Oliva-Urcia et al., 2009*).

In this paper we present new AMS data and field observations from asymmetric folds located in the South-Central Pyrenees and developed in different lithologies (carbonates, shales, siltstones and marls). The folds were formed during the Variscan and/or Pyrenean orogenies and six of them show a macroscopic tectonic foliation due to the mechanisms of pressure-solution. The comparison of the AMS data coming from both limbs with field observations will contribute to better describe the evolution of folding, hence to clarify the interplay of deformational mechanisms that took place in these Pyrenean folds.

2. Geological setting

Two main orogenies are recognizable in the Pyrenees, the Variscan and the Alpine, also called Pyrenean. The Variscan orogeny is indentifiable in the Pyrenean Axial Zone (PAZ) by the remnants of the collision between Gondwana and Laurassia during Middle Devonian to Permian times *(Ziegler, 1990; Matte, 2001)*. The Alpine fold-and–thrust-belt developed when Africa collided with Eurasia from the late Cretaceous to the Miocene (*Muñoz, 1992*). It is the main cause for the present day configuration of the Pyrenean Mountain Range. Our study focuses on seven folds located in different thrust sheets of the south-central Pyrenees. Three of them are developed in Paleozoic rocks, hence affected by both orogenies, and four folds in Eocene rocks, affected only by the Pyrenean orogeny, (Figs. 1.a, 1.b, 2 and 4a, Table 1).

The PAZ is the Variscan internal core of the Alpine double vergent Pyrenean Range. It is characterized by an asymmetrical south verging antiform, constituted by the stacking of thrust sheets of Variscan rocks unconformably overlain by a discontinuous cover of post-Variscan rocks *(Séguret, 1972; Muñoz, 1992)*. The outcropping thrust sheets are from top to bottom Gavarnie, Orri and Rialp (Fig. 1.b). Internal deformation of these Alpine thrust-sheets is moderate to weak, and is mostly linked to the reactivation of Variscan structures (*Gil-Peña, 2004* among others). Traditionally, two structural domains have been differentiated in PAZ, the infrastructure and the suprastructure (*Zwart, 1963*). The study area locates in the suprastructure which is generally characterized by subvertical to south verging folds with associated cleavage development in a low grade metamorphism environment. Most of the tectonic foliations and folds observed in the Variscan rocks are Variscan in age. Alpine thrusts are responsible for the general doming and tilting of the Variscan structures and localized deformation along the Alpine thrust sheet zones (*Ábalos et al., 2002*). However, no evidence of alpine penetrative structures has been found in the sampled folds. The observed deformational structures in the Variscan rocks are related to the Variscan deformation imprint (*García-Sansegundo, 2004; Gil-Peña, 2004*), and hence, AMS results will reflect the Variscan poliphase (or not) deformation.

The South Pyrenean Zone (SPZ) is situated to the south of the Axial Zone. The structure of the SPZ in the west-central part of the Pyrenees is controlled by south verging thrust sheets and related folds. The older cover thrust sheets are the imbricated system of Larra-Monte Perdido, Lutetian-Bartonian in age *(Séguret, 1972; Teixell, 1992),* which affects Upper Cretaceous-Eocene rocks and roots to the north with the Lakora basement thrust sheet in the west (*Teixell, 1996*). This imbricated system is later affected by foreland breaking sequence basement thrusts (Gavarnie, Bielsa and Guarga) active from Eocene to Oligocene *(Labaume et al., 1985; Teixell, 1992; Martínez-Peña and Casas-Sainz, 2003),* Fig. 4b. The transition between the aforementioned sector of the SPZ in the west and the South Pyrenean Central Unit (SPCU) (*Séguret, 1972*) in the east is an area where N-S striking folds affect Mesozoic to Eocene outcropping rocks. The thrust sheets of the SPCU are from north to south Bóixols, Montsec and Serres Marginals and affect the Cenozoic sedimentary rocks in a foreland breaking sequence from Late Cretaceous to Oligocene times *(Vergés and Muñoz, 1990; Muñoz, 1992; Muñoz et al., 2013)*. The N-S striking folds (Arro system, Boltaña, Añisclo, Balzes anticlines, located at the western side of the SPCU, not shown in figures) are interpreted to be related to lateral ramps of the Montsec and the Serres Marginals thrust sheets (SPCU) and their development is related to the Mesozoic sedimentary thickness variation along strike (among other factors) *(Soto et al., 2002; Soto et al., 2006)*.

The migration to the west of the deformation of the Montsec thrust affects the syntectonic deposits in the area (*Soto et al., 2002; Martínez-Peña and Casas-Sainz, 2003; Tavani et al., 2006)*. The Montsec thrust sheet is part of the foreland sequence thrusts detached over Triassic evaporites in the SPCU. The N-S orientation of these folds is related to clockwise rotation (from 32º to 80º), paleomagnetically documented in the western termination of the SPCU *(Dinarès-Turell, 1992; Fernández-Bellón, 2004; Mochales, 2012; Muñoz et al., 2013; Rodríguez-Pintó et al., 2016)*. Rotations in nearby areas to the southwest in the External Sierras (*Pueyo et al., 2002*) and west in the Internal Sierras *(Oliva-Urcia and Pueyo, 2007; Izquierdo-Llavall et al., 2015*) are also found.

3. Structural observations

3.1. Folds developed in Paleozoic rocks

Three folds affecting the Paleozoic rocks were selected: Erta (ER), Manyanet (MANY) and Ars (ARS) folds. They are localized in the south central area of the Pyrenean Axial Zone (Fig. 1, Tables 1 and 2) and are developed on Devonian (ER and MANY) or Upper Ordovician (ARS) non- to very low-grade metamorphic rocks. These three structures form asymmetric Variscan folds with a complex polyphase and poly-orogenic evolution *(Carreras and Capella, 1994; García-Sansegundo et al., 2011)*. In the area where the studied folds are located, two main Variscan deformation phases and their associated structures have been described (D1 and D2, *Mey, 1968*). The first deformation phase (D1) caused a large south verging fold and thrust belt, locally related to cleavage *(Mey, 1968; de Sitter, 1959; Gil-Peña and Barnolas, 2001; 2004)*. The second deformation phase (D2) caused ESE-WNW south verging folds and thrusts, linked to a well-defined foliation *(Mey, 1968; Poblet, 1991; García-Sansegundo et al., 2011)*. The structural superimposition of these two deformation phases produced a complex interference folding pattern (recognized as type 2 according to Ramsay, 1967 in Erta and Manyanet folds), characterized in the field by the lithological contrast between the Silurian (shales) and the Devonian (dominated by limestones) (Fig. 2 and sketch of Fig. 4a).

The three folds are situated in the Orri thrust sheet (Orri dome), an Alpine structure developed by the reactivation of the plurikilometric D1 helvetic-type Orri nappe (*Gil-Peña, 2004*), detached onto the Silurian shales. The ARS fold is developed in the siliciclastic, thinning-upwards, Upper Ordovician sequence, which interlayers a carbonate unit in its upper part. The cores were sampled in the siltstones of the Upper Ordovician Cava Formation (Fm) (*Hartevelt, 1970*). The fold is a decametric to hectometric scale cylindrical D2 anticline, whose axis is trending E-W (284º, 09º). It has a rounded hinge area with a subvertical to north dipping overturned south limb and a south dipping to subhorizontal normal limb and a slaty axial planar cleavage dipping around 45º N. The sampled bed has a class 1C geometry (*Ramsay, 1967*). The ARS fold developed at the footwall of the D2 Variscan Llavorsí thrust, onto the weakly deformed normal limb of the Orri nappe (*Gil-Peña and Barnolas, 2004*).

The ER and MANY folds developed in Devonian rocks. ER fold is a refolded Variscan fold cored in the shales and limestones of the Lower Devonian Rueda Fm *(Mey, 1968; Sanz-López, 2004)*; Fig. 1.b. It shows a type 2 interference pattern (*Ramsay, 1967*) resulting from the superimposition of a syn-main Variscan cleavage fold (D2) trending WSW-ENE onto a D1 south verging gently inclined anticline. ER fold outcrops in the hangingwall of the Erta nappe, a Variscan south verging structure, related to the D1 event, with a presently, southern dipping attitude. The fold is fossilized by the Stephano-Permian and Triassic rocks. Minor fractures in these rocks are associated to a slight reactivation of the Erta nappe in fragile mode during the Alpine times. The axial planar foliation related to D1 is slaty to spaced, with variable orientations. The foliation related to D2 is not obvious in the sampled outcrop, although regionally it shows a WNW orientation, with dips between 45º and 60º to the North. However, this WNW orientation is oblique to the D2 fold orientation (WSW-ENE) deduced from the interference pattern in map view (*Mey, 1968*). Parasitic D1 folds measured on the overturned limb are plungig towards the SW 15-55º (Table 2). Samples for the AMS study were collected in the shaly limestones from the Castanesa limestone Fm and in the calcareous slates of the Fonchanina Fm.

The MANY fold is a decametric to hectometric scale structure, developed in the limestones with interbedded argillaceous limestones and shales of the Lower Devonian Manyanet Fm. This fold is a southeast verging antiformal syncline, with long limbs and a bulbous tight hinge area trending to collapse. It is associated to an axial planar continuous to anastomosed spaced cleavage, developed during D1. This cleavage is angularly folded in the steeper northern limb by D2 (MANY1), processed favored by the refraction of cleavage in the multilayer system. However, in the southern limb (MANY2) S1 exhibits a sigmoidal geometry closer to the bedding plane (as described in *Ham and Bell, 2004*). The MANY fold represents a second order Z-fold (*Ramsay and Huber, 1987*) developed in the overturned limb of the plurikilometric D1 south-verging Variscan Orri nappe. Its present axial plunge (030, 12) results from a refolding by D2.

3.2 Folds developed in Eocene rocks

The four asymmetric studied folds affecting Eocene rocks are situated in the Central sector of the South Pyrenean Zone (SPZ) (Figs 1.a, 1c, 3, 4b and Table1). Their development is related to the evolution of the Pyrenean Mountain Range during the Alpine orogeny (from Upper Cretaceous to Miocene times. The folds Salarons (SA), Ordesa (ORD) and Sta. Elena (ELE) are decametric anticlines with a Pyrenean orientation (ENE-WSW) and the Metils fold (MMM) is a kilometric syncline with a N-S orientation. SA and ORD represent examples of the Larra-Monte Perdido fold- and thrust imbricated system and affect the Nummulite Marls (Gallinera Fm, Ilerdian; *van Lunsen, 1970; Teixell, 1992)*. ELE has a Pyrenean orientation and is a metric scale fold affecting Lutetian turbiditic deposits *(van Lunsen, H., 1970; Labaume et al., 1985)* of the Jaca-Pamplona basin. It is related to the emplacement of the Larra-Monte Perdido cover thrust and Gavarnie basement thrust (*Teixell, 1996*). A regional cleavage is associated to the emplacement of this basement thrust *(Choukroune and Séguret, 1973; Labaume et al., 1985; Teixell, 1992; 1996; 1998; Izquierdo-Llavall et al., 2013; Rodríguez et al., 2014)*. The cleavage affects all folds developed in Eocene rocks and its orientation mostly follows the main structural directions. This cleavage is axial planar to meso-scale folding in most of the SPZ (*Izquierdo-Llavall et al., 2013*). Notwithstanding the sampled siltstone layer in ELE fold does not show macroscopically the development of this regional tectonic foliation as occurs in the other folds, nearby pelite layers do show the macroscopic development of cleavage planes (tilted ~ 60º towards the N).

The N-S trending MMM syncline is located in the western limb of the Añisclo anticline, which is related to the Montsec thrust sheet *(Tavani et al., 2006; Muñoz et al., 2013)* and it develops in the Metils Marls Fm (*van Lunsen, H., 1970*). It also shows the preservation of a regional cleavage *(Holl and Anastasio, 1995*). The MMM fold is part of the Sobrarbe fold system *(Fernández-Bellón, 2004),* 2004), a fold system of detachment and fault-propagation folds deforming the Upper Cretaceous-Paleogene rocks of the Gavarnie thrust sheet, at the footwall of the Montsec thrust sheet, dated as Paleocene-late Ypresian and rooted to basement thrusts in the Axial Zone (*Séguret, 1972*).

The three ENE-WSW folds are asymmetric with the northern limb (long/normal limb) gently dipping to the north and a strongly north dipping overturned or vertical southern limb (short limb). The N-S oriented fold (MMM) has the eastern limb almost vertical and the western limb gently dipping to the southwest.

4. Rock magnetic study

4.1. Technical aspects

Different carbonate and siliciclastic lithologies (marls, siltstones, shales and carbonatic rocks) of the sampled sites were selected to carry out magnetic mineral analyses, namely the temperature dependence of susceptibility and of the induced magnetization. The samples were analyzed from -194 to 15°C for their magnetic susceptibility (κ–T) in a KLY-4S Kappabridge (working at 300 A/m and 875 Hz) combined with a CS-L/CS-3 apparatus (AGICO Inc.) at the University of Karlsruhe. From room temperature to 700 °C we used the KLY-4S Kappabridge equipment at the University of Karlsruhe and a KLY-3S Kappabridge equipment combined with a CS-3 furnace at the University of Zaragoza. Heating/cooling rates ranged between 3–4 and 11–14 °/min for the low and high temperature runs respectively. Measurements were performed in an argon atmosphere in order to avoid mineral reactions with oxygen during heating (flow rate of 100 ml/min). The raw data were corrected for the empty cryostat/furnace and normalized. The percentage of the ferromagnetic original content has been calculated considering the ferromagnetic behaviour of the heating curve, as a straight horizontal line *(Hrouda, 1994*). Low temperature curves (between -195 and 0ºC) enhance the hyperbolic behaviour characteristic of the paramagnetic phase following the Curie-Weiss law $k_{para} = C/T\text{-}\theta$ (where k_{para} is the paramagnetic susceptibility, C is the Curie constant, T is the temperature, and θ the paramagnetic Curie temperature.

In addition, 17 samples were analysed in a Variable Field Translation Balance (VFTB) (Petersen Instruments), at the University of Burgos. Acquisition of isothermal remanent magnetization (IRM), back field, hysteresis loops (up to 0.8 Tesla) and thermomagnetic curves measuring the variation of an induced magnetization at ~37 mT with temperature were performed in the Curie Balance on powder samples (< 450 mg).

4.2. AMS

Magnetic susceptibility (κ) is a physical property of solids and represents the capacity of the material to be magnetized (M) in a given magnetic field (H), M = κ x H. This property is anisotropic (*Nye, 1957*) and the anisotropy of magnetic susceptibility (AMS) is described as a second-rank tensor. AMS in rocks depends primarily on crystallographic preferred orientation, shape fabric of grains, composition, magnetic interactions between grains and, to lesser extent, on distribution and size of microfractures (*Tarling and Hrouda, 1993*).

Three axes define the susceptibility ellipsoid: maximum (k_{max}), intermediate (k_{int}) and minimum (k_{min}). Their orientations correspond to the eigenvectors of the susceptibility tensor. Other parameters give information about the shape and degree of magnetic fabric development (*Jelinek, 1981*): the magnetic lineation ($L = k_{max}/k_{int}$), magnetic foliation ($F = k_{int}/k_{min}$), the corrected anisotropy degree, *P'* (intensity of the preferred orientation of minerals), and T shape parameter, varying between -1 and +1, prolate shapes for T<0 and oblate shape for T>0. The principal axes of the ellipsoid are also displayed on stereographic projection using *Stereonet 3.4* (*Cardozo and Allmendinger, 2013*, and *Allmendinger et al., 2013)*. The Woodcok diagram represents two ratios of the three eigenvalues of the magnetic ellipsoid (E1>E2>E3) on a natural logarithmic scale, therefore, clustering of the k_{max} and k_{min} axes is visualized in the Woodcock diagram (*Woodcock, 1977*). In this type of graph, the division line for uniaxial clusters and great-circle girdles distributions is k=1. Uniaxial clusters plot where E2 = E3, i.e., along the line ln (E2/E3) = 0. Axially symmetric plot where E1 = E2, i.e. along the line ln (E1/E2) = 0. The C values are a measurement of the strength of the preferred orientation *(Parés et al., 1999; Larrasoaña et al., 2004)*.

A total of 14 sites were investigated for the study of the AMS. Sites are distributed in pairs at each limb of seven asymmetric folds. The AMS measurements (7 to 11 specimens per site) were performed on a susceptibility bridge (Kappabridge KLY-3S (AGICO Inc.) at the University of Zaragoza), by inserting the sample in 3 different positions and using the rotator, working at AC (875 Hz and 300 A/m). The deviatoric susceptibility tensor is computed after the measurements. The Kappabridge KLY-2.03 (Geofyzika Brno) of the University of Barcelona was used by measuring 15 directional susceptibilities at a frequency of 920 Hz. Sensitivity of the measurement is about 5 x 10^{-7} SI and the matrix elements and individual errors are calculated following *Jelinek (1977; 1981)*.

5. Results

5.1. Rock magnetism

The sampled sites are located in the same lithological level except for ER fold, where the closest levels were sampled. Samples from the same fold show similar values of the bulk magnetic susceptibility Km, which can be an indication of the ferromagnetic fraction (*Hirt et al., 2008*).

Magnetic susceptibility versus temperature curves are irreversible and indicate the dominance of paramagnetic minerals as susceptibility carriers, with percentages ranging from 60 % (carbonates and shales) to 95 % (marls, shales) (calculated with cureval software, AGICO Inc.) except for two cases (ER1 and ELE6 with 40 and 45% content of paramagnetic minerals respectively). The calculations take into account the hyperbolic behavior of the curve when paramagnetic minerals dominate (following the Curie-Weiss law), and subtract a constant ferromagnetic content also obtained from the curve (*Hrouda, 1994*). However, mineral reactions take place during heating despite the argon atmosphere, as seen in the variation of the magnetic susceptibility with respect to the temperature (Figs. 5a and b, left column). A ferromagnetic phase is formed during heating, marked by an increase in magnetic susceptibility before the Curie temperature (Tc) of magnetite (Tc: 580ºC) between 400º and 580ºC (Fig. 5). The cooling run from 700ºC to 40ºC indicates the presence of magnetite. The increase in magnetic susceptibility with heating has been related to mineral alteration of for example, clay minerals (*Roberts and Pillans, 1993*). The induced magnetization variation respect to temperature and hysteresis loops from the VFTB, Petersen Instruments (Figs. 5 a and b, central and right columns) also show neo-formation of magnetite during the heating procedure (Curie temperature at about 580 ºC) and the predominance of a paramagnetic carrier, respectively.

5.2. AMS

The magnetic parameters: P', T and Km values are presented in Table 3 and Figs. 6a and 6b for the Paleozoic rocks and Figs. 7a and 7b for the Eocene rocks.

The mean values of the corrected anisotropy degree (P') represent the eccentricity of the magnetic ellipsoid and vary from 1.012 (MANY1) to 1.122 (ARS11). The average value of the shape parameter (T) shows contrasting values depending on the age of the rock; for the Paleozoic rocks, the overturned (short) limbs are oblate and the normal (long) limbs are prolate, whereas in the Eocene rocks the overturned (short) limbs are prolate (except SA2) and the normal (long) limbs are oblate. The mean values of Km vary from 35.7 x 10^{-6} SI (ER1) to 421 x 10^{-6} SI (ARS11) and most sites have bulk susceptibilities between 150 and 400 x 10 $^{-6}$ SI corresponding to paramagnetic values, as confirmed with the k-T curves. The lack of linear correlation between Km and P' also confirm that variation of the corrected anisotropy degree is not related to the mineral composition. These observations support the interpretation of the AMS in terms of mineral preferred orientation (petrofabric).

Orientation distribution of magnetic susceptibility axes

The Woodcock diagram allows to differentiate the distribution of the maximum and minim axes of the magnetic ellipsoid, showing that for the Paleozoic rocks, the overturned (short) limbs show a larger scattering of k_{max} axes (Figs. 6c). The clustering of the k_{min} axes is not so clear, although two folds show a better clustering in the long limb (Fig. 6d).

The orientation of the magnetic susceptibility ellipsoid is presented in Table 4 and stereoplots of Figs. 6e. In the Paleozoic sites, the k_{min} axes overlap with the pole to the cleavage plane in the short limbs of MANY and ER and in the long limb of ARS. The k_{max} axes lie on the cleavage plane in ER and ARS). This orientation is characteristic of a tectonic fabric, which is a modified fabric due to tectonic events also responsible for the development of tectonic foliation or cleavage. The best example of tectonic fabric are ARS sites, where a significant orientation difference can be seen between cleavage and bedding planes. However, only three samples in the overturned (short) limb of ARS (ARS11) are oriented with respect to the bedding plane, that is, k_{min} axes cluster closed to the pole of the bedding plane. However, the location of the k_{max} axes of those three samples is tectonically modified since they are located close to the intersection lineation of the bedding and cleavage planes. This orientation of AMS axes is common in rocks that register only one main compressional event *(Parés et al., 1999) Borradaile and Henry, 1997; Borradaile and Jackson, 2004; Oliva-Urcia et al., 2009)*. Generally, ARS and MANY sites do not show the k_{max} axes at the intersection lineation (between bedding and cleavage planes). In ER sites, cleavage and bedding planes are almost parallel, however, in the long limb, k_{max} axes concentrate around the second order D1 fold axes measured in field.

In the Eocene rocks, according to the Woodcock diagram, the girdle distribution of the k_{max} axes is predominant in the overturned (short) limb (except for MMM1), whereas the k_{min} axes show a good clustering for all sites except for MMM1 (Figs. 7c and 7d). With respect to the orientation of the axes (Table 4, Fig. 7e), ORD1, 2, SA1, 2 and MMM2 sites show also a tectonic fabric with the k_{min} axes cluster near the pole to the cleavage plane. The clustering of the k_{max} axes in the intersection lineation only occurs in MMM2 (normal/long limb). On the contrary, in MMM1, with a clear prolate shape, the k_{max} is clustered on the bedding plane (not in the intersection lineation). The ELE sites show a similar dis-orientation regardless the bedding or cleavage planes orientation.

6. Discussion

The petrofabric obtained in both limbs of seven asymmetric folds by means of the anisotropy of the magnetic susceptibility (AMS) together with field structural observations give clues about the mechanisms operating during folding, since the modification of the magnetic fabric from deposition to the final magnetic fabric unravel the deformation evolution. The folds selected for this study show a variety of lithology, size, geometry and structural position inside the architecture of the Southern Pyrenees and their deformation history. However, the same layer (or equivalent for ER sites) in each fold has been sampled for AMS analyses to compare the petrofabric of both limbs in order to minimize the effect of variations in the magnetic mineralogy on the magnetic fabric. The rock magnetic analyses indicate that paramagnetic minerals are the main carriers of the magnetic fabric.

The mechanisms of internal deformation in parallel folding are flexural flow and tangential longitudinal strain (*Ramsay, 1967*). Flexural flow means that strain is concentrated on limbs and no strain occurs on bedding planes but slip, and when slip planes are more widely spaced, the layer-parallel shearing would be concentrated along bedding planes (i.e., flexural slip fold, *Price and Cosgrove, 1990*). Tangential longitudinal strain (TLS) has strain concentrated in the hinges of the fold. These two mechanisms can be accompanied by a variable degree of pure shear (flattening) (*Ramsay, 1967*). The flexural flow mechanism seems to occur in the alpine folds, as interpreted from field observations and the AMS analyses (see below). Another folding mechanism is shear folding. The folding mechanisms are difficult to disentangle from the final deformed rock. In addition, as deformation evolves, folds can be refolded (with the same mechanisms mentioned above) but their geometry may appear as parasitic folds. The conditions that result in parasitic folding in multilayer systems depend on the different combinations of thicknesses and viscosities of their layers, (*Treagus and Fletcher, 2009; Hudleston and Treagus, 2010* and references there in). In practice, refolding is strongly conditioned by previous structure and is mechanically more difficult when folds of the two phases are non-coaxial (*Watkinson and Cobbold, 1981*). Hence, low dipping planar features (bedding and/or foliation) of the early folds will be easily refolded or crenulated by subsequent phases of deformation, while high dipping planar features will be more probably rotated. *Ham and Bell (2004)* showed the continuous reactivation of foliations during folding, and how subsequent phases of deformation affect limbs differently, i.e., which limb shears vs. develops an oblique new cleavage by rotating the earlier formed oblique foliation into parallelism with S0//S1. These mechanisms (flexural, shear folding and flattening) seem to occur in the Variscan folds as interpreted from field observations and AMS analyses (see below).

Variscan folds

In the case of the Variscan folds, we have compared the normal and the overturned limbs of a helvetic-type *nappe* developed during the first Variscan deformational phase (D1) through the investigation of their second order structures ER and MANY, which are located in the frontal-lateral area of the *nappe* (Fig. 2b). Figs. 4a, 9). The second Variscan deformational phase (D2) refolded these D1 structures. On the other hand, the second deformation phase (D2) is studied with the ARS fold since in these structure, D1 internal deformation is negligible (Fig. 4). The Alpine deformational imprint on this folds is subtle in this area and it is characterized by the antiformal stack of thrust sheets with shear deformation within the thrust planes and tilting of previous structures. However, no internal Alpine penetrative deformation within the thrust sheets themselves is observed (*Mey 1968, García-Sansegundo, 2004; Gil-Peña, 2004*).

A general observation is drawn from the comparison of the magnetic fabric between the two limbs, there is a higher scattering of the k_{max} axes in the overturned (short) limbs (Fig. 6c; MANY1, ER2, ARS11), than in the normal (long) limb. This shape of the magnetic ellipsoid is oblate in the overturned (short) limb, contrary to the prolate geometry obtained in the normal (long) limb. The shape parameter (*Parés et al., 1999* and references therein) and distribution of the maximum and minimum axes of the magnetic ellipsoid in the Woodcock diagram (*Woodcock, 1977*) has been used to differentiate degrees of deformation in weakly deformed mudrocks (folded and with pencil structures), therefore, deformation increases with girdling of the k_{min} axes and clustering of k_{max} axes (*Larrasoaña et al., 2004*) and with increasing eccentricity of the magnetic ellipsoid, shape of the magnetic ellipsoid changes from oblate to prolate to oblate again (*Parés et al., 1999*). However, shape parameter and degree of anisotropy has found to be related to the value of the angle between cleavage and bedding planes in low-grade pelitic rocks, with higher angles between cleavage and bedding planes, the magnetic ellipsoid is more prolate and shows a lower degree of anisotropy. These differences are related to the mineral carriers of the magnetic fabric (*Debacker et al., 2004; 2009*). Similarly, larger eccentricity parameters of the magnetic ellipsoid were found in the limbs with respect to the hinge of small-scale folds in Banded Iron Formations (*Mukherji et al., 2004*). In the case of the Variscan folds, only ARS show high angle between bedding and cleavage planes, whereas in MANY2 and ER sites, cleavage and bedding are parallel or almost parallel.
For strongly deformed rocks as the ones in this study, with two phases of cleavage development during the Variscan orogeny in two cases, the Woodcock diagram has to be reassessed.

To consider the possible changes in the orientation of the magnetic ellipsoid through the Variscan orogeny, ARS sites are the starting scenario, since ARS is a D2 fold developed on the non-deformed long limb of the D1 Orri nappe. The magnetic fabric in ARS shows a typical tectonic fabric (*Borradaile and Henry, 1997*), with k_{max} and k_{int} axes on the tectonic foliation plane and k_{min} axes clustered around the pole to the tectonic foliation plane, although only in the normal (long) limb and few samples of the overturned (short) limb, the k_{max} axes cluster near the intersection lineation. The few samples clustered near the intersection lineation in ARS overturned (short) limb result in a higher eccentricity of the magnetic oblate ellipsoid (P') for that limb. Considering the classical view of shape/eccentricity and degree of clustering of magnetic axes, the results are contradictory, since girdling of k_{min} axes and eccentricity would suggest a higher degree of deformation in the overturned (short), whereas the low clustering of k_{max} axes indicates the contrary. The higher deformation degree in the overturned (short) limb would be expected in a flexural flow deformation mechanism since simple shear is expected to be more intense in that limb.

The refolded Erta anticline (ER) shows a consistent magnetic fabric with well-clustered axes, which is not surprising considering the parallelism between bedding and cleavage planes. An interchange between k_{min} and k_{int} axes in the normal (long) limb (ER1), that is, the k_{int} axes are clustered around the pole to the bedding plane leaving the k_{min} axes located near the bedding plane the most prolate magnetic ellipsoid of all Variscan folds. In addition, the k_{max} axes in ER1and ER2 lie near parallel to the second order D1 fold axis. The orientation of the clustered k_{max} axes is close to the maximum dipping direction of the bedding//cleavage plane, which is a consequence of the doming of D1 folds by D2 structures. This could indicate that in the ER fold, in spite of the general obliquity between D1 and D2, stretching due to D2 refolding parallels the D1 phase. Therefore, both deformations in this case, flexural flow and shear folding, add, reinforcing a common stretching direction. The stretching due to D2 seems to be more intensive in the 'external' normal limb (ER1) of the D2 structure and it will explain why ER1 develops a prolate magnetic fabric. Shear mechanism involved in the formation of the D1 ER fold would do expectable a high angle between the axis of D1 minor folds and the k_{max} axes, which is not seen. Considering the classical view of shape/eccentricity and degree of clustering of magnetic axes, the results are contradictory, since shape/eccentricity would suggest a higher degree of deformation in the overturned (short) limb, whereas the clustering of the magnetic axes indicates the contrary (for the classical view of the Woodcock diagram for weakly deformed mudrocks).

In the Manyanet fold (MANY), the magnetic fabric of the overturned (short) limb (MANY1) is weakly defined, in contrasts with the well-defined fabric in the normal (long) limb (MANY2). This reflects a different behaviour of folding respect to the Erta fold during the D2 refolding phase. This observation is clear at outcrop scale where in the short limb (MANY1) the originally low dipping cleavage (in green in Fig. 4 and Fig. 9) has been folded by D2 structures (Figs. 2a, 4). However, in the gently dipping limb (MANY2) the originally steep cleavage rotates to be almost parallel to the bedding plane. Despite the cleavage development, k_{max} axes are still on the bedding plane. Some samples show the k_{min} axes on the bedding plane, indicating an interchange with the k_{int} axes (at the pole of the bedding plane) probably due to the similar magnitude of both axes in the prolate magnetic ellipsoid, as it occurs in ER1 (equivalent long limb in D2). However, the magnetic fabric in MANY1 shows the petrofabric due to the folded cleavage, and, as this is not a penetrative feature, the resulting ellipsoids become highly scattered. The successive deformation events result in a better definition of the magnetic fabric in the long limb of the fold, probably due to a flattening in that limb, whereas flattening in the short limb results in S1 folding which in turns provokes a scattering of the magnetic ellipsoid exes.

The XY plane obliquity with respect to bedding is a function of layer competence. When a high competence contrast occurs between adjacent levels, it results in a marked refraction of cleavage (MANY1). During the D2 deformation event, the short limb rotates, what results in the amplification of S1 refraction by folding of the cleavage. S1 folding is favored by switching from layer parallel shortening to stretching because of rotation with increasing fold amplification. Deformation accommodates then in the hinge area, where TLS folding is accompanied by some degree of inner arc volume loss through pressure-solution mechanism (hinge collapse). In the short limb (MANY1) the new XY plane becomes the axial plane of the folded D1 cleavage. This new XY plane results almost parallel to bedding, and x axis will follow the dip direction of such plane. Therefore, the two ellipsoids of D1 and D2 are non-coaxial, since the one related with D1 is oblique to bedding and the one related to D2 is parallel to bedding. We interpret the petrofabric (and hence the magnetic fabric) as a sum up of two different folding mechanisms (shear folding and flattening) as in Erta, and the final result will depend on the orientation and geometry in every position of the structure. In the MANY2 long limb, S1 forms to a low angle with So. D2 deformation rotates S1 planes into parallelize with So, reinforcing the original fabric. The interchange of k_{min} and k_{int} axes in the normal/long limb of ER and MANY is a common feature that seems unrelated to the magnetic mineralogy (Fig. 5a). In both limbs D1 and D2 cleavages show a similar orientation and are oblique to bedding. The superposition of deformational events seems to produce a rotation of the prolate ellipsoid, leaving the k_{min} axes in the cleavage plane and the k_{int} axes perpendicular to the cleavage plane. This interchange of axes does not occur in ARS, where apparently only D2 affects the Cambro-Ordovician rocks (Fig. 9). The k_{max} axes in ER and MANY plunge to the S (ER1 and ER2 to the SW, and MANY2 to the SE, in response to its position in the reverse limb of the D1 Orri nappe) what could be related with the general southward emplacement of the Variscan nappes (D1) and thrusts (D2) and the southward tilting of these structures by Alpine orogeny.

The clustering of k_{max} axes as seen in the Woodcock diagram of the Variscan folds would suggest a higher degree of flattening in the normal (long) limbs for strongly deformed rocks by poliphase events.

Pyrenean folds

In the folds developed in the Eocene rocks 3 out of 4 overturned (short) limbs (except MMM1) show a higher scattered distribution of the k_{max} axes with respect to their normal limbs, as it happens in the folds developed in Paleozoic rocks (Figs. 6 and 7), and ELE6 is close to an isotropic distribution. In the case of the Pyrenean folds, this observation is explained by the superposition of different magnetic fabrics due to the evolution of the deformation. Looking at the temporal relationship between folding and cleavage, three of the sampled structures developed prior to the regional alpine cleavage, which later overprints these structures (SA, ORD and MMM) and only ELE is folded while regional alpine cleavage develops (Priabonian to Rupelian times*, Labaume et al., 1985; Teixell, 1992; Izquierdo-Llavall et al., 2013)*. From a geometrical point of view, cleavage is coherent with the folds when it is observed on their normal limbs. Therefore, the XY plane of the strain ellipsoid for the normal limb is parallel to the cleavage (Fig. 9). This observation implies that cleavage superposition to the folding 'reinforces' the original tectonic fabric of the fold, and hence the magnetic fabric. However, as both mechanisms are coaxial it is not possible to differentiate if the magnetic fabric is the result of only one deformative event (cleavage development) or if some limb deformation (typically by flexural flow) had previously accommodated the deformation in the fold. On the contrary, in the overturned limb, the inferred ellipsoid linked to folding with limb deformation is oblique to the deformation ellipsoid defined by cleavage (Fig. 9). Consequently, when cleavage overprints an overturned limb with flexural flow or flexural slip, the addition of both ellipsoids will be a new ellipsoid that only will share one axis (x or y). This suggests that the scattering of the axes in the short limb is related to the deformation in the limb of the fold prior to cleavage development and therefore the petrofabric show the remains of the first tectonic developed fabric (related to folding due to Larra-Monte Perdido imbricated thrust system).

The large scattering in both limbs of ELE is probably related to grain size and carbonatic content of the sampled layer, being higher than in the other Eocene folds, which indicates lower content of phyllosilicates and a poorer definition of the magnetic fabric.

7. Conclusions

The analyses of seven asymmetric folds developed in Paleozoic and Eocene rocks in the Axial and the South Pyrenean Zone respectively by means of the anisotropy of magnetic susceptibility and structural field observations allows deciphering how the internal deformation during folding affects the petrofabric. The AMS, carried mainly by the paramagnetic fraction, reflects the sum of the different tectonic phases (D1 and D2) and mechanisms (flexural, shearing, TLS, flattening) in the case of the Paleozoic rocks, and folding and cleavage development (flexural folding mechanism and flattening) in the case of the Eocene rocks with the total obliteration of the original sedimentary fabric. The folded layers show a tectonic fabric with k_{max} axes on the cleavage plane and k_{min} or k_{int} at the pole to the cleavage plane (except in ELE, MMM and MANY1), and generally, sites in the overturned (short) limb show a higher scattering of magnetic axis and higher eccentric magnetic ellipsoid respect to the corresponding normal (long) limb.

Coaxiality of Variscan deformation phases D1 and D2 is deduced in the Paleozoic rocks for ER overturned site, and non-coaxiality for MANY overturned site due to a more intensive degree of shear deformation during D1 in the reversal limb of the Helvetic type Orri nappe (represented by the MANY fold) than in the normal limb (represented by ER fold). In MANY the higher scattering in the short limb is related to the folding of the first cleavage plane (related to D1 and due to flattening) respect to an axial plane that is the second cleavage (developed with D2). This folding of cleavages does not occur in the long limb, but a rotation of cleavage planes, which get parallel to So. The parallelism in the long limbs of ER and MANY folds between bedding and D2 cleavage planes results in a prolate ellipsoid, suggesting a higher flattening deformation than in the short limb. The petrofabric in the Eocene rocks also show a tectonic orientation and a higher scattering of the magnetic lineation in the overturned limb suggesting a superposition and coaxiality in the normal limb of the flexural flow deformation related to folding with the strain related to the cleavage development (XY plane). This is not happening in the overturned limb, where flexural flow and shear folding deformation do not overlap, therefore the folding fabric related to the Larra-Monte Perdido thrust system remains scattered. The Woodcock diagram of the k_{max} axes allows differentiate the degree of flattening within the same folded layer for strongly deformed rocks by poliphase deformational events in a similar fashion than for the degree of deformation in weakly deformed rocks. The Woodcock diagram of the k_{min} axes is not conclusive in the studied cases.

Acknowledgements

BOU is thankful for the free use of the instruments of the different Universities (Karlsruhe in Germany and Zaragoza, Burgos in Spain) and the Unit of CCiTUB-CSIC in Barcelona. Financial support came from the Spanish Ministry of Science and Innovation - FEDER Funds (MICINN) and from the National Parks Organism, Spain. Geotransfer Research Group of the University of Zaragoza is acknowledged for logistics and fruitful discussions. We acknowledge the comments of anonymous reviewers and Prof. M. Mamtami which help to improve the manuscript.

REFERENCES

Ábalos, B., Carreras, J., Druguet, E., Escuder-Viruete, J., Gómez-Pugnaire, M.T., Lorenzo-Álvarez, S., Quesada, C., Rodríguez-Fernández, L.R., Gil-Ibarguchi, I., 2002. Variscan and Pre-Variscan Tectonics., in: *The Geology of Spain*, Geological Society of London. pp. 179–182.

Alfonsi, L., 1997. Paleomagnetic and anisotropy of magnetic susceptibility (AMS) analyses of the Plio-Pleistocene extensional Todi Basin, central Italy. *Annals of Geophysics*, 40.

Allmendinger, R.W., Cardozo, N.C., Fisher, D., 2013. Structural Geology Algorithms: Vectors & Tensors. Cambridge, England, Cambridge University Press.

Amrouch, K., Beaudoin, N., Lacombe, O., Bellhasen, N., Daniel, J.M., 2011. Paleostress magnitudes in folded sedimentary rocks. *Geophysical Research Letters*, 38.

Anderson, M.W., Morris, A., 2004. The puzzle of axis-normal magnetic lineations in folded low-grade sediments (Bude Formation, SW England). *Geological Society, London, Special Publications*, 238, 175–190.

Aubourg, C., Rochette, P., Bergmüller, F., 1995. Composite magnetic fabric in weakly deformed black shales. *Physics of the Earth and Planetary Interiors*, 87, 267–278.

Borradaile, G., 1987. Anisotropy of magnetic susceptibility: rock composition versus strain. *Tectonophysics*, 138, 327–329.

Borradaile, G.J., 1988. Magnetic susceptibility, petrofabrics and strain. *Tectonophysics*, 156, 1–20. doi:10.1016/0040-1951(88)90279-X

Borradaile, G.J., Henry, B., 1997. Tectonic applications of magnetic susceptibility and its anisotropy. *Earth Sciences Reviews*, 42, 49–93.

Borradaile, G.J., Jackson, M., 2004. Anisotropy of magnetic susceptibility (AMS): magnetic petrofabrics of deformed rocks. *Geological Society, London, Special Publications*, 238, 299–360. doi:10.1144/GSL.SP.2004.238.01.18

Borradaile, G.J., Tarling, D.H., 1981. The influence of deformation mechanisms on magnetic fabrics in weakly deformed rocks. *Tectonophysics*, 77, 151–168.

Cardozo, N.C., Allmendinger, R.W., 2013. Spherical projections with OSXStereonet. *Computers and Geosciences*, 51, 193–205.

Carreras, J., Capella, I., 1994. Tectonic levels in the Paleozoic basement of the Pyrenees: a review and a new interpretation. *Journal of Structural Geology*, 16, 1509–1524.

Choukroune, P., Séguret, M., 1973. Carte Structurale des Pyrénées, 1/500.000, Université de Montpellier – ELF Aquitaine.

Cifelli, F., Mattei, M., Chadima, M., Hirt, A.M., Hansen, A., 2005. Cifelli, F., Mattei, M., Chadima, M., Hirt, A. M., & Hansen, A. (2005). The origin of tectonic lineation in extensional basins: combined neutron texture and magnetic analyses on “undeformed” clays. *Earth and Planetary Science Letters*, 235(1), 62-78. Earth and Planetary Science Letters 235, 62–68.

de Sitter, L.U., 1959. de Sitter, L.U., 1959. The structure of the axial zone of the Pyrenees in the province of Lérida. *Estudios Geológicos*, 15, 349-360.

Debacker, T. N., Hirt, A. M., Sintubin, M., and Robion, P., 2009. Differences between magnetic and mineral fabrics in low-grade, cleaved siliciclastic pelites: A case study from the Anglo-Brabant Deformation Belt (Belgium). *Tectonophysics*, 466, 32–46.

Debacker, T.N., Robion, P., Sintubin, M., 2004. The anisotropy of magnetic susceptibility (AMS) in low-grade, cleaved pelitic rocks: influence of cleavage/bedding angle and type and relative orientation of magnetic carriers. *Geological Society, London, Special Publications*, 238, 77–107.

Dinarès-Turell, J., 1992. Paleomagnetisme a les Unitats Sudpirinenques Superiors. Implicacions estructurals. PhD. Universidad de Barcelona. 462 pp.

Donath, F.A., Parker, R.B., 1964. Folds and folding. Geological Society of America Bulletin, 75(1), 45-62. Geological Society of America Bulletin 75, 45–62.

Escher, A., Watterson, J., 1974. Stretching fabrics, folds and crustal shortening. Tectonophysics 22, 223–231.

Fernández-Bellón, Ó., 2004. *Reconstruction of geological structures in 3D:an example from southern Pyrenees*. PhD., Universidad de Barcelona, 321pp.

García-Lasanta, C., Roman-Berdiel, T., Oliva-Urcia, B., Casas, A.M., Gil-Peña, I., Speranza, F., Mochales, T., 2016. Tethyan versus Iberian extension during the Cretaceous period in the eastern Iberian Peninsula: insights from magnetic fabrics. *Journal of the Geological Society*, 173(1), 127-141. Journal of the Geological Society 173, 127–141.

García-Sansegundo, J. (2004). Estructura varisca en los Pirineos, In: Geología de España (J. Vera, Ed.); SGE- IGME. Madrid. Pp. 254 – 258.

García-Sansegundo, J., Poblet, J., Alonso, J.L., 2011. García-Sansegundo, J., Poblet, J. Clariana, P., Alonso, J.L., 2011. Hinterland-foreland zonation of the Variscan orogen in the Central Pyrenees: comparison with the north portion of the Iberian Variscan Massif. In: Poblet, J. and Lisle, R. (eds.), Kinematic evolution and structural styles of fold-and-thrust belts. Geological Society Special Publication 349, 169-184., in: *Kinematic Evolution and Structural Styles of Fold-and-Thrust Belts*. Geological Society Special Publication, p. 169–184.

Ghosh, S.K., 1966. Experimental tests of buckling folds in relation to strain ellipsoid in simple shear deformations. *Tectonophysics,* 3, 169–195.

Gil-Peña, I., 2004. Estructura alpina de la zona axial., in: *Geología de España*. SGE-IGME, Madrid, pp. 323–325.

Gil-Peña, I., Barnolas, A., 2004. El Domo del Orri (Pirineo central): un pliegue-manto reactivado por la tectónica alpina. *Geotemas,* 6, 267–270.

Gil-Peña, I., Barnolas, A., 2001. Superposición estructural hercínica y alpina en el borde occidental del domo de Pallassos (Noguera de Tor, Pirineo central). *Boletín Geológico y Minero*, 112, 5–16.

Graham, J.W., 1966. Significance of Magnetic Anisotropy in Appalachian Sedimentary Rocks, in: Steinhart, J.S., Smith, T.J. (Eds.), *Geophysical Monograph Series.* American Geophysical Union, Washington, D. C., pp. 627–648.

Graham, J.W., 1954. Magnetic susceptibility anisotropy, an unexploited petrofabric element. *Geological Society of America Bulletin*, 65, 1257–1258.

Ham, A.P., Bell, T.H., 2004. Recycling of foliations during folding. *Journal of Structural Geology*, 26, 1989–2009.

Hartevelt, J.., 1970. *Geology of the Upper Segre and Valira valleys, Central Pyrenees, Andorra/Spain*. Sheet 10, 1: 50.000. Leidse Geologische Mededelingen 45, 167–236.

Hirt, A.M., Schmidt, V., Almquist, B.S.G., 2008. Understanding magnetic fabrics. Geotectonic Research 95, 65–67.

Holl, J.E., Anastasio, D.J., 1995. Cleavage development within a foreland fold and thrust belt, southern Pyrenees, Spain. *Journal of Structural Geology,* 17, 357–369.

Housen, B.A., van der Pluijm, B.A., 1990. Chlorite control of correlations between strain and anisotropy of magnetic susceptibility. *Physics of the Earth and Planetary Interiors*, 61, 315–323.

Housen, B.A., Richter, C., van der Pluijm, B.A. (1993). Composite magnetic anisotropy fabrics: experiments, numerical models, and implications for the quantification of rock fabrics. *Tectonophysics*, 220, 1–12.

Hrouda, F., 1994. Hrouda, F. (1994). A technique for the measurement of thermal changes of magnetic susceptibility of weakly magnetic rocks by the CS-2 apparatus and KLY-2 Kappabridge. Geophysical Journal International, 118(3), 604-612. *Geophysical Journal International*, 118, 604–612.

Hrouda, F., 1987. Mathematical model relationship between the paramagnetic anisotropy and strain in slates. *Tectonophysics*, 142, 323–327.

Hrouda, F., 1982. Magnetic anisotropy of rocks and its application in geology and geophysics. *Geophysical Surveys*, 5, 37–82. doi:10.1007/BF01450244

Hudleston, P.J., Treagus, S.H., 2010. Information from folds: a review. *Journal of Structural Geology,* 32, 2042–2071.

Izquierdo-Llavall, E., Casas-Sainz, A.M., Oliva-Urcia, B., 2013. Heterogeneous deformation recorded by magnetic fabrics in the Pyrenean Axial Zone. *Journal of Structural Geology,* 57, 97–113.

Izquierdo-Llavall, E., Casas-Sainz, A.M., Oliva-Urcia, B., Burmester, R., Pueyo, E.L., Housen, B.A., 2015. Izquierdo-Llavall, E., Sainz, A. C., Oliva-Urcia, B., Burmester, R., Pueyo, E. L., & Housen, B. (2015). Multi-episodic remagnetization related to deformation in the Pyrenean Internal Sierras. *Geophysical Journal International*, 201(2), 891-914.

Jackson, M., 1991. Anisotropy of magnetic remanence: A brief review of mineralogical sources, physical origins, and geological applications, and comparison with susceptibility anisotropy - Springer. *Pure and Applied Geophysics,* 136, 1–28.

Jamison, W.R., 1987. Geometric analysis of fold development in overthrust terranes. *Journal of Structural Geology,* 9, 207–219.

Jelinek, V., 1981. Characterization of the magnetic fabric of rocks. *Tectonophysics,* 79, 63–70.

Jelinek, V., 1977. *The statistical Theory of Measuring Anisotropy of Magnetic Susceptibility of Rocks and its Application*. Geofyzika, Brno, 88 pp.

Kadzialko-Hofmokl, M., Mazur, S., Wermer, T., Kruczyk, J., 2004. Relationships between magnetic and structural fabrics revealed by Variscan basement rocks subjected to heterogeneous deformation—a case study from the Kłodzko Metamorphic Complex, Central Sudetes, Poland. *Geological Society, London, Special Publications,* 238, 475–491.

Kligfield, R., Owens, W.H., Lowrie, W., 1981. Magnetic susceptibility anisotropy, strain, and progressive deformation in Permian sediments from the Maritime Alps (France). *Earth and Planetary Science Letters,* 55, 181–189. doi:10.1016/0012-821X(81)90097-2

Kneen, N.S., 1976. The relationship between the magnetic and strain fabrics of some hematite-bearing Welsh slates. *Earth and Planetary Science Letters*, 31, 413–416.

Labaume, P., Séguret, M., Seyve, C., 1985. Evolution of a turbiditic foreland basin an analogy with an accretionary prism: Example of the Eocene South-Pyrenean basin. *Tectonics,* 4, 661–685.

Larrasoaña, J.C., Pueyo-Morer, E.L., Parés, J.M., 2004. An integrated AMS, structural, paleo- and rock-magnetic study of Eocene marine marls from the Jaca-Pamplona Basin (Pyrenees, N Spain): New insights into the timing of magnetic fabric acquisition in weakly deformed mudrocks., in: *Magnetic Fabric: Methods and Applications*, Geological Society, London, Special Publ. Geological Society, London, Special Publ., pp. 127–143.

Lüneburg, C.M., Lampert, S.A., Lebit, H.D., Hirt, A.M., Casey, M., Lowrie, W., 1999. Magnetic anisotropy, rock fabrics and finite strain in deformed sediments of SW Sardinia (Italy). Tectonophysics, 307(1), 51-74. *Tectonophysics*, 307, 51–74.

Martínez-Peña, M.B., Casas-Sainz, A.M., 2003. Cretaceous–Tertiary tectonic inversion of the Cotiella Basin (southern Pyrenees, Spain). *International Journal of Earth Sciences,* 92, 99–113.

Mamtani, M.A., Sengupta, P., 2010. Significance of AMS analysis in evaluating superposed folds in quartzites. *Geological Magazine*, 147, 910–918.

Mamtani, M.A., Greiling, R.O., Karanth, R.V., Merh, S.S., 1999. Orogenic deformation and its relationship to AMS fabric—an example from the southern margin of the Aravalli Mountain Belt, India. In: Radhakrishna, T., Piper, J.D. (Eds.), The Indian Subcontinent and Gondwana: a Palaeomagnetic and Rock Magnetic Perspective, Geological Society of India Memoir, 44: 9–24

Matte, P., 2001. The Variscan collage and orogeny (480–290 Ma) and the tectonic definition of the Armorica microplate: a review. *Terra Nova*, 13, 122–128.

Mattei, M., Sagnotti, L., Faccena, C., Funiciello, R., 1997. Mattei, M., Sagnotti, L., Faccenna, C., & Funiciello, R. (1997). Magnetic fabric of weakly deformed clay-rich sediments in the Italian

peninsula: relationship with compressional and extensional tectonics. *Tectonophysics*, 271(1), 107-122. Tectonophysics 271, 107–122.
Mey, P.H.W., 1968. *Geology of the Upper Ribargozana and Tor valleys, Central Pyrenees, Spain*. Sheet 8, 1: 50.000.
Mochales, T.; Casas, A.M.; Pueyo, E.L.; Barnolas, A., 2012).Rotational velocity for oblique structures (Boltaña anticline, southern Pyrenees). *Journal of Structural Geology* 35, 2-16.
Mukherji, A., Chaudhuri, A.K., Mamtani, M.A., 2004. Regional scale strain variations in the Banded Iron Formations of Eastern India: results from anisotropy of magnetic susceptibility studies. J. Struct. Geol. 26, 2175–2189.
Muñoz, J.A., 1992. Evolution of a continental collision belt: ECORS-Pyrenees crustal balanced cross-section., in: *Thrust Tectonics*. Springer Netherlands, pp. 235–246.
Muñoz, J.A., Beamud, E., Fernández, Ó., Arbués, P., Dinarés-Turell, J., Poblet, J., 2013. The Ainsa Fold and thrust oblique zone of the central Pyrenees: Kinematics of a curved contractional system from paleomagnetic and structural data. *Tectonics*, 32, 1142–1175.
Nye, J.F., 1957. *Physical Properties of Crystals*. Oxford Univ. Press, Oxford.
Oliva-Urcia, B., 2004. *Geometría y Cinemática rotacional en las Sierras Interiores y Zona Axial (sector de Bielsa) a partir del análisis estructural y paleomagnético*. Zaragoza. 290pp.
Oliva-Urcia, B., Larrasoaña, J.C., Pueyo, E.L., Gil, A., Mata, P., Parés, J.M., Schleicher, A.M., Pueyo, O., 2009. Disentangling magnetic subfabrics and their link to deformation processes in cleaved sedimentary rocks from the Internal Sierras (west central Pyrenees, Spain). *Journal of Structural Geology*, 31, 163–176.
Oliva-Urcia, B., Pueyo, E.L., 2007. Rotational basement kinematics deduced from remagnetized cover rocks (Internal Sierras, southwestern Pyrenees). *Tectonics*, 26.
Oliva-Urcia, B., Román-Berdiel, T., Casas, A.M., Bógalo, M.F., Osácar, M.C., García-Lasanta, C., 2013. Transition from extensional to compressional magnetic fabrics in the Cretaceous Cabuérniga basin (North Spain). *Journal of Structural Geology*, 46, 220–234.
Parés, J.M., van der Pluijm, B.A., Dinarès-Turell, J., 1999. Evolution of magnetic fabrics during incipient deformation of mudrocks (Pyrenees, northern Spain). *Tectonophysics*, 307, 1–14.
Poblet i Esplugas, J., 1991. *Estructura herciniana i alpina del vessant sud de la zona axial del Pirineu central*. Universidad de Barcelona.
Price, N.J., Cosgrove, J.W., 1990. *Analyses of Geological Structures*. Cambridge University Press.
Pueyo, E.L., Millán, H., Pocoví, A., 2002. Rotation velocity of a thrust: a paleomagnetic study in the External Sierras (Southern Pyrenees). *Sedimentary Geology*, 146, 191–208.
Ramberg, H., 1964. Selective buckling of composite layers with contrasted rheological properties. *Tectonophysics*, 1, 307–341.
Ramberg, H., 1963. Fluid dynamics of viscous buckling applicable to folding of layered rocks. *Bulletin of the American Association of Petroleum Geologists*, 47, 484–505.
Ramsay, J. G., Huber, M. I., 1987. *The techniques of modern structural geology: Folds and fractures* (Vol. 2). Academic press.
Ramsay, J.G., 1967. *Folding and fracturing of rocks*. McGraw-Hill Companies.
Rathore, J.S., Henry, B., 1982. Comparison of Strained Magnetic Fabrics in Dalradian Rocks from the Southwest Highlands of Scotland. *Journal of Structural Geology*, 4, 373–384.
Roberts, A.P., Pillans, B.J., 1993. Rock magnetism of lower/middle Pleistocene marine sediments, Wanganui basin, New Zeland. *Geophysical Research Letters*, 20: 839-842.
Rodríguez, L., Cuevas, J., Tubía, J.M., 2014. Structural Evolution of the sierras interiores (Aragón and Tena Valleys, South Pyrenean Zone): tectonic implications. *The Journal of Geology*, 122, 99–111.
Rodríguez-Pintó, A., Pueyo, E.L., Calvín, P., Sánchez, E., Ramajo, J., Casas, A.M., Ramón, M.J., Pocoví, A., Barnolas, A., Román, T., 2016. Rotational kinematics of a curved fold: a structural and paleomagnetic study in the Balzes anticline (Southern Pyrenees). *Tectonophysics*, 677–678, 171–189.
Sanz-López, J., 2004. *Silúrico, Devónico y Carbonífero pre- y sin-varisco de los Pirineos*., in:

Geología de España. SGE-IGME, Madrid, pp. 250–254.
Séguret, M., 1972. *Étude tectonique des nappes et séries décollées de la partie centrale du versant sud des Pyrénées: caractère synsédimentaire, rôle de la compression et de la gravité*. Publications de l'Université des sciences et techniques du Languedoc (USTELA).
Soto, R., Casas, A.M., Storti, F., Faccenna, C., 2002. Role of lateral thickness variations on the development of oblique structures at the Western end of the South Pyrenean Central Unit. *Tectonophysics*, 350, 215–235.
Soto, R., Larrasoaña, J.C., Arlegui, L., Beamud, E., Oliva-Urcia, B., Simón, J.L., 2009. Reliability of magnetic fabric of weakly deformed mudrocks as a palaeostress indicator in compressive settings. Journal of Structural Geology, 31(5), 512-522. *Journal of Structural Geology*, 31, 512–522.
Soto, R., Storti, F., Casas-Sainz, A.M., 2006. Impact of backstop thickness lateral variations on the tectonic architecture of orogens: insights from sandbox analogue modelling and application to the Pyrenees. *Tectonics,* 25. doi:10.1029/2004TC001693
Stone, D.B., 1962. Anisotropic magnetic susceptibility measurements on a phonolite and on a folded metamorphic rock. *Geophysics,* 62, 375–380.
Suppe, J., 1985. Principles of structural geology. Prentice Hall.
Tarling, D.H., Hrouda, F., 1993. *Magnetic anisotropy of rocks*. Springer Science & Business Media.
Tavani, S., Storti, F., Fernández, Ó., Muñoz, J.A., Salvani, F., 2006. Tavani, S., Storti, F., Fernández, O., Muñoz, J. A., & Salvini, F. (2006). 3-D deformation pattern analysis and evolution of the Anisclo anticline, southern Pyrenees. *Journal of Structural Geology*, 28(4), 695-712. Journal of Structural Geology 28, 695–712.
Teixell, A., 1998. Crustal structure and orogenic material budget in the west central Pyrenees. *Tectonics,* 17, 395–406.
Teixell, A., 1996. The Ansó transect of the southern Pyrenees: basement and cover thrust geometries. *Journal of the Geological Society* 153, 301–310.
Teixell, A., 1992. *Estructura alpina en la transversal de la terminación occidental de la Zona Axial pirenaica*. Tesis doctoral. Universitat de Barcelona. 252pp.
Treagus, S.H., Fletcher, R.C., 2009. Controls of folding on different scales in multilayered rocks. *Journal of Structural Geology*, 31, 1340–1349.
van Hise, 1894. *Principles of North American Precambiaran Geology*. US Geol. Surv. Am. Rep. 16, 581–843.
van Lunsen, H., 1970. *Geology of the Ara-Cinca region, Spanish Pyrenees, Province of Huesca*. Thesis Utrecht, Geologica Ultraiectina.
Vergés, J., Muñoz, J.A., 1990. Thrust sequence in the southern central Pyrenees. *Bulletin de la Societé géologique de France*, 6, 265–271.
Watkinson, A.J., Cobbold, P.R., 1981. Axial directions of folds in rocks with linear/planar fabrics. *Journal of Structural Geology,* 3, 211–217.
Woodcock, N.H., 1977. Specification of fabric shapes using an eigenvalue method. *Geological Society of America Bulletin,* 88, 1231–1236.
Ziegler, P.A., 1990. Collision related intra-plate compression deformations in Western and Central Europe. *Journal of Geodynamics,* 11, 357–388.
Zwart, H.J., 1963. The structural evolution of the Paleozoic of the Pyrenees. *Geol. Rundschau*, 53, 170 – 205.

Table 1a. Location of the studied sites, Geographic coordinates (UTM), bedding (So) orientation, indication of fold limb: Long (normal) or Short (overturned or vertical) and tectonic foliation (S1) orientations

		UTM (E-W)	UTM (N-S)	So (Strike, Dip and Dip Direction)	Long/Short limb	S1 (Strike, Dip and Dip Direction)
MANY-1	31T	327055	4701693	062, 88 S	S	057,74 N/081, 70 S
MANY-2	31T	327055	4701693	032, 24 S	L	028, 49 S
ER-1	31T	322573	4699114	170, 37 W	L	168, 39 W
ER-2	31T	322518	4699113	175, 21 W	S	174, 23 W
ARS11	31T	366147	4699964	100, 90	S (near hinge)	090, 52 N
ARS12	31T	366151	4699947	096, 44 S	L	088, 39 N
ELE6	30T	719102	4723288	077, 86 N	L	103, 57 N
ELE7	30T	719102	4723288	153, 20 NE	S	103, 57 N
MMM1	31T	259567	4711690	170, 80 W	L	163, 45 E
MMM2	31T	258466	4713498	145, 40 W	S	166, 49 E
ORD2	30T	744901	4729189	098, 68 N	L	117, 22 N
ORD1	30T	744901	4729189	100, 11 N	S	110, 32 N
SA2	30T	740354	4728927	088, 22 N	L	111, 37 N
SA1	30 T	740382	4728990	125, 38 N	S	095, 36 N

Table 1b. Summarized description of the folds, age, lithology, type* (after Ramsay, 1967 and van Hise, 1894), main deformation event, thrust sheet location/main deformation event and tectonic foliation (for more details, see text)

	Name	Age/Lithology	Type*. Main deformation event	Thrust sheet location /Main deformation phase/tectonic foliation
Variscan	MANY	Devonian argillaceous limestones (Manyanet Fm), carbonates/marls	Minor fold in second order Z-fold* (antiformal syncline). D1 variscan fold refolded by D2.	Overturned limb of D1 fold, refolded by D2 (anastomosed cleavage of D1 folded in steeper limb)
	ER	Devonian black shales and carbonatic shales (Castanesa and Fonchanina Fms), shales	Type 2* interference (D2 onto D1)	Hangingwall of Erta nappe (D1). Reactivation in alpine. D1 slaty tectonic foliation with variable orientation, unclear D2 tectonic foliation (45-60º N)
	ARS	Upper Ordovician, Cava Fm, siltstones	Cylindrical D2 anticline	At the footwall of Variscan Llavorsi thrust (normal limb of Orri napppe). Tectonic foliation dipping to the N
Alpine	ELE	Eocene (Lutetian) Turbidites (competent layer: siltstone)	Similar*	Larra-Monte Perdido cover thrust and Gavarnie basement thrust. Tectonic foliation dipping to the N
	MMM	Eocene (Ilerdian). Metils Marls Fm	Similar*	Montsec thrust sheet. Tectonic foliation dipping to the E
	ORD	Eocene (Ilerdian) Gallinera Fm, marls	Similar*	Larra-Monte Perdido cover thrust. Tectonic foliation dipping to the N
	SA	Eocene (Ilerdian). Gallinera Fm, marls	Similar*	Larra-Monte Perdido cover thrust. Tectonic foliation dipping to the N

Table 2. Orientation of minor fold axis and crenulations in the Palezoic folds

	E1 (axes of minor folds)	**Lcr** (crenulation, l2)	Thrusting towards S or SW
ER1 (long/normal)	236, 35 242, 56	330, 05	Overlapped type 2. Regionally, Orri nappe detaches towards S-SSW, with a curved axis of the helvetic nappe, and both ER and MANY are located in a lateral zone of the nappe. Originally, D1 fold axes would be oriented with an inmersion towards the NW. The D2 emplacement direction of the thrust sheets is also S-SSW, but previous deformation leaves the beds oblique to the new transport direction, the D1 fold axes scatter with D2.
ER2 (short/reverse)	228, 35 209, 32 191, 14 258, 16	072, 10	
MANY2 (long)	030, 12 112, 16 (D2)		
MANY1 (short)	---		
ARS	284, 09		

Table 3. Mean values of the magnetic ellipsoid parameters. Magnetic lineation (L), magnetic foliation (F), corrected anisotropy degree (P’), shape parameter (T) and bulk susceptibility. s.d.: Standard deviation.

	Long/Short limb	**L**	s.d.	**F**	s.d.	**P'**	s.d.	**T**	s.d.	**$K_{mean}(10^{-6})$SI**	s.d.
ER1	L	1.021	0.010	1.012	0.004	1.034	0.014	-0.224	0.201	35.696	7.379
ER2	S	1.038	0.004	1.069	0.017	1.112	0.017	0.257	0.167	291.133	8.138
MANY1	S	1.005	0.002	1.007	0.004	1.012	0.004	0.064	0.388	103.751	21.196
MANY2	L	1.022	0.009	1.020	0.005	1.043	0.015	-0.035	0.088	213.388	51.012
ARS11	S (near hinge)	1.043	0.018	1.074	0.007	1.122	0.013	0.279	0.237	420.890	19.807
ARS12	L	1.036	0.007	1.034	0.010	1.072	0.008	-0.030	0.196	389.920	6.930
ELE6	L	1.013	0.004	1.008	0.004	1.022	0.004	-0.235	0.335	109.976	12.192
ELE7	S	1.004	0.002	1.009	0.001	1.013	0.002	0.414	0.137	138.880	75.100
MMM1	L	1.022	0.006	1.008	0.003	1.031	0.007	-0.480	0.226	255.090	57.546
MMM2	S	1.014	0.005	1.034	0.008	1.050	0.009	0.418	0.197	168.160	18.450
SA1	S	1.028	0.007	1.039	0.020	1.071	0.017	0.071	0.304	169.120	17.491
SA2	L	1.009	0.005	1.074	0.011	1.092	0.013	0.777	0.129	195.860	5.308
ORD1	S	1.016	0.004	1.019	0.004	1.037	0.001	0.079	0.241	286.419	83.636
ORD2	L	1.026	0.008	1.025	0.009	1.052	0.007	-0.044	0.291	243.108	16.054

Table 4. AMS directional data

Bingham distribution (eigenvector orientation – azimuth and inclination of E1, E2 and E3– and eigenvalue –[E1], [E2] and [E3] –) at every site of k_{max}, k_{int} and k_{min}.

	kmax						*kint*						*kmin*					
	E1	**|E1|**	**E2**	**|E2|**	**E3**	**|E3|**	**E1**	**|E1|**	**E2**	**|E2|**	**E3**	**|E3|**	**E1**	**|E1|**	**E2**	**|E2|**	**E3**	**|E3|**
ER1	226.44	0.9595	131.06	0.0307	35.46	0.0097	47.45	0.9502	315.02	0.0400	223.45	0.0098	317.01	0.9300	51.83	0.0542	227.07	0.0158
ER2	247.17	0.9791	153.14	0.0205	25.68	0.0005	341.11	0.9813	249.11	0.0162	117.74	0.0025	102.70	0.9929	226.12	0.0050	319.17	0.0021
MANY1	149.19	0.5832	27.57	0.2952	249.26	0.1215	169.70	0.4463	62.06	0.3656	330.19	0.1881	264.29	0.5208	18.36	0.3991	146.41	0.0801
MANY2	145.30	0.9789	343.59	0.0141	240.08	0.0070	281.53	0.8531	40.2	0.1353	142.29	0.0115	43.21	0.8547	292.43	0.1395	151.39	0.0058
ARS 11	94.18	0.8501	263.72	0.1441	3.03	0.0058	344.38	0.8379	248.08	0.1497	248.51	0.0124	194.41	0.8620	30.48	0.1291	291.08	0.0089
ARS 12	58.50	0.9603	320.07	0.0261	224.39	0.0136	297.22	0.9737	71.59	0.0220	199.20	0.0043	193.30	0.9796	51.54	0.0172	295.18	0.0032
ELE6	72.63	0.8958	213.22	0.0937	310.16	0.0105	231.25	0.8120	345.41	0.1539	119.39	0.0340	322.06	0.8755	228.34	0.1003	60.55	0.0090
ELE7	120.45	0.7834	225.15	0.2077	328.41	0.0089	216.07	0.7713	115.59	0.2195	310.31	0.0092	216.41	0.9655	49.04	0.0292	144.49	0.0404
MMM1	201.63	0.9527	291.00	0.0251	21.27	0.0112	307.07	0.7507	39.16	0.2251	194.72	0.0242	40.29	0.7684	304.10	0.2174	196.59	0.0142
MMM2	167.11	0.9604	72.25	0.0233	278.63	0.0163	64.48	0.9680	162.07	0.0243	257.41	0.0077	40.29	0.7684	142.34	0.0200	27.32	0.0061
SA1	351.46	0.8268	88.07	0.1518	184.43	0.0214	93.13	0.8186	357.28	0.1756	205.59	0.0058	194.45	0.9573	104.00	0.0331	14.46	0.0096
SA2	307.12	0.6037	45.33	0.3886	200.54	0.0077	43.28	0.5998	312.03	0.3951	217.62	0.0051	205.59	0.9758	18.31	0.0139	110.03	0.0103
ORD1	45.35	0.9655	297.23	0.0208	181.46	0.0137	313.03	0.9668	223.06	0.0305	68.84	0.0027	219.56	0.9708	92.22	0.0202	351.24	0.009
ORD2	48.54	0.7287	144.04	0.2372	237.36	0.0341	304.08	0.6905	47.59	0.2256	209.30	0.0839	216.35	0.8565	319.19	0.1032	73.49	0.0404

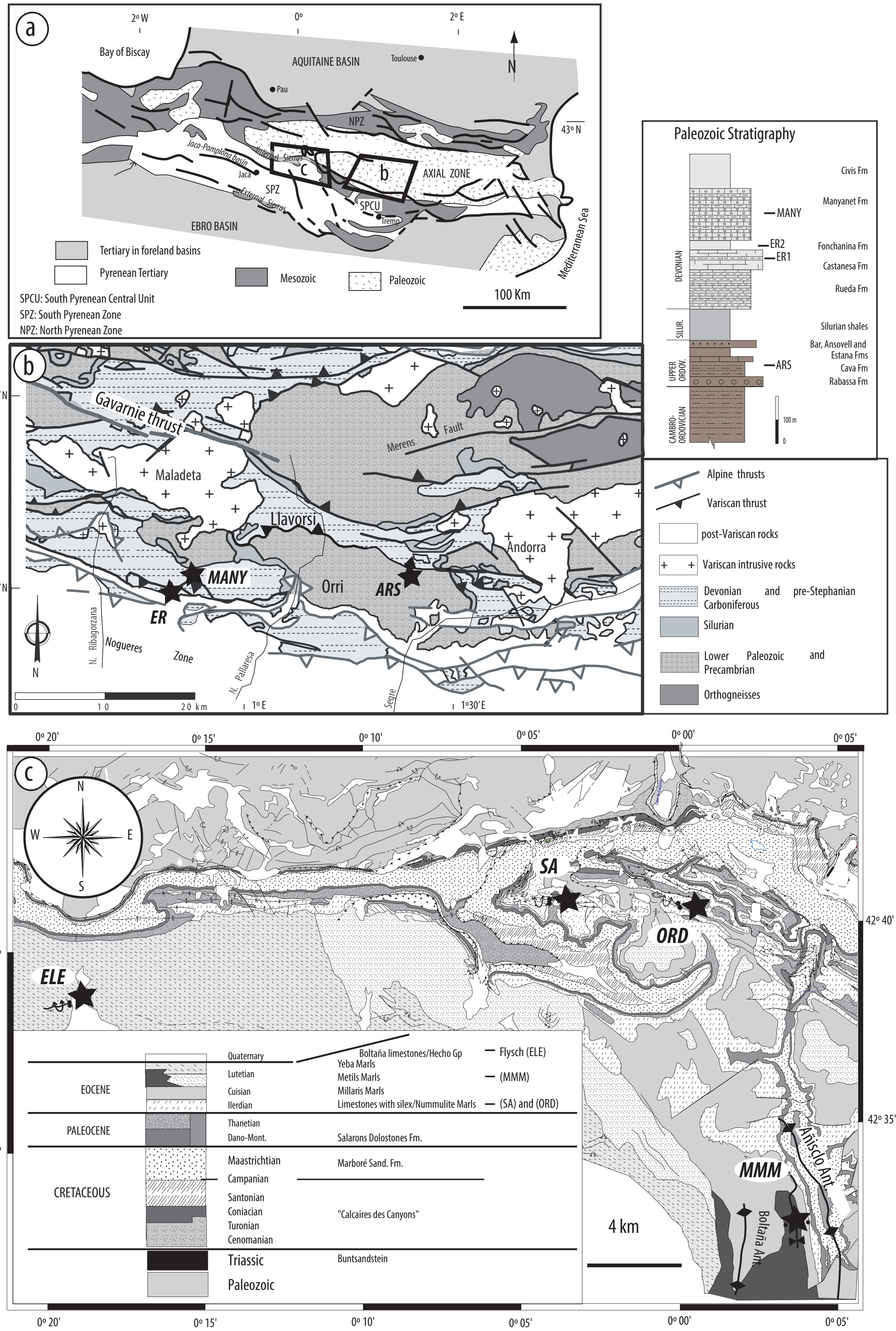

FIG. 1. Oliva-Urcia et al.

Fig. 1. a) General map of the Pyrenees; b) detailed geological map of the Paleozoic folds and stratigraphy; c) detailed geological map of the Eocene folds (simplified from Oliva-Urcia, 2004).

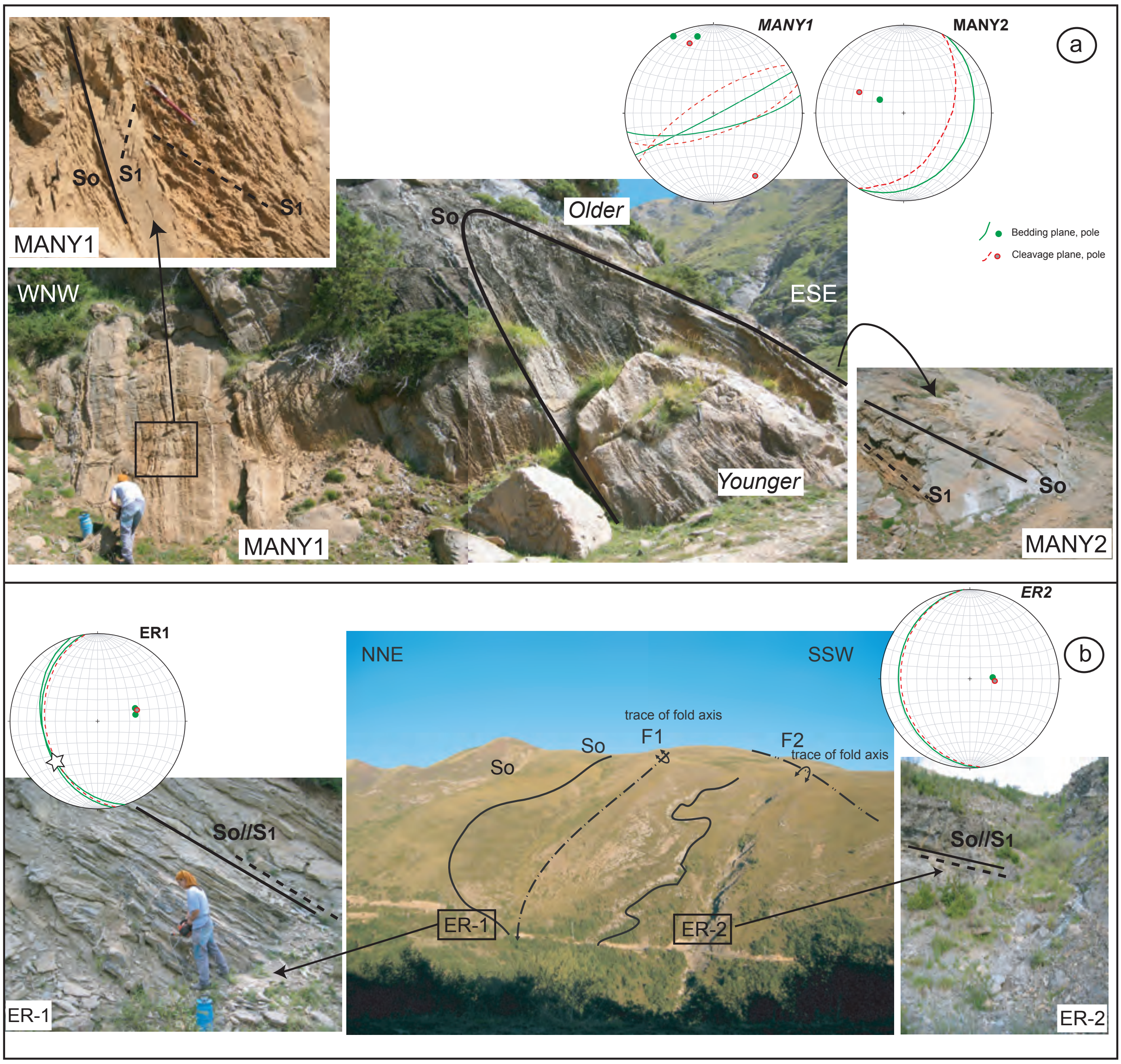

Fig. 2. Field pictures of Paleozoic folds. a) Manyanet (MANY); b) Erta (ER). Stereoplots show geographic projection of bedding and cleavage (plane and pole). In ER1 stereoplot, the star represents the stretching direction measured in the field. S_0: bedding orientation; S_1: tectonic foliation orientation; F1: D1 deformation trace of fold axis; F2: D2 deformation trace of fold axis.

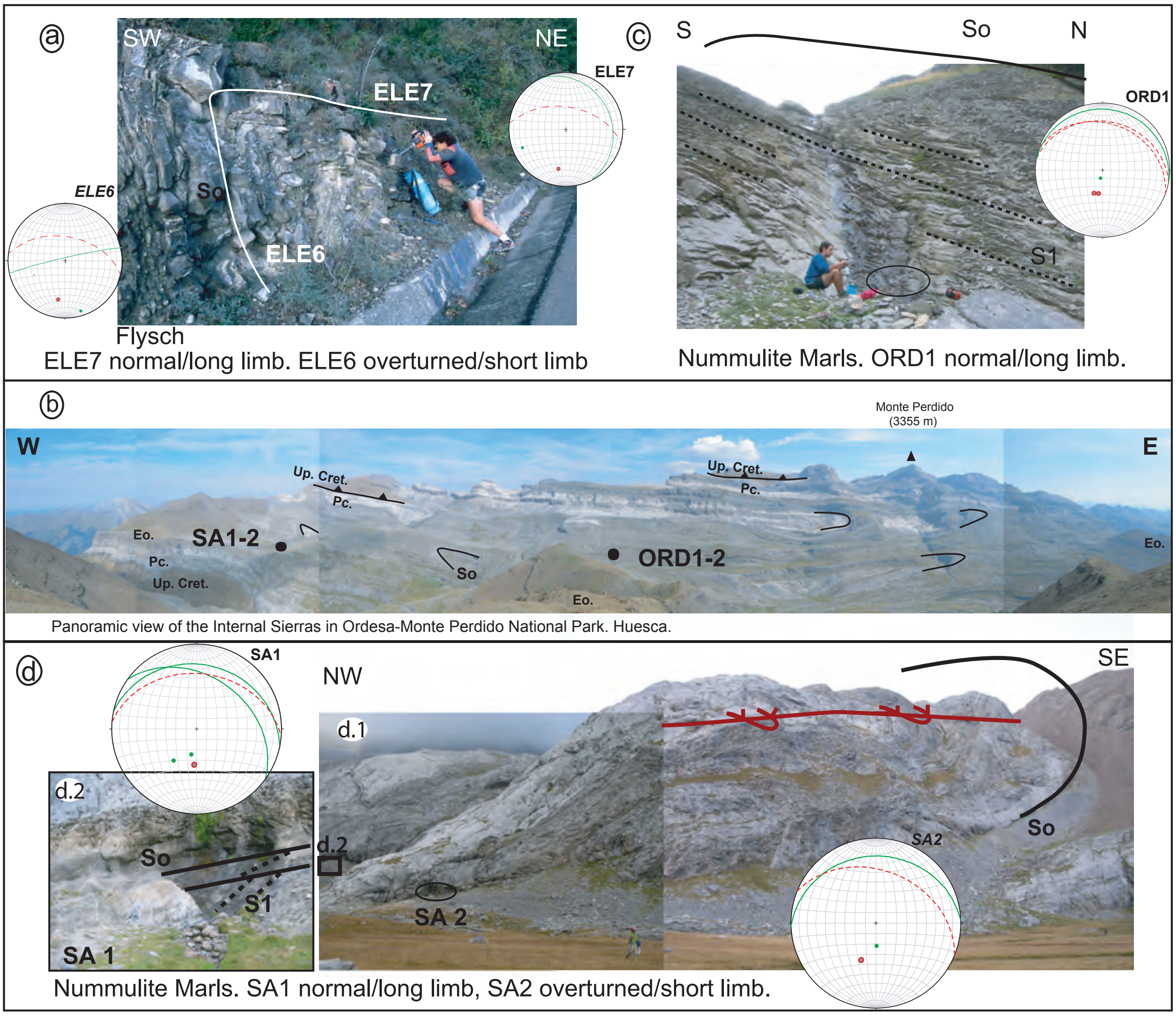

Fig. 3. Field pictures of Eocene folds. A) Metric scale anticline in turbidites of the Jaca-Pamplona basin. Flysh, ELE7: normal/long limb, ELE6: overturned/short limb. b) General view of the Internal Sierras (Ordesa-Monte Perdido National Park), where folds related to the Larra-Monte Perdido imbricated thrust system are shown. Up Cret: Upper Cretaceous, Pc: Paleocene, Eo: Eocene. Dashed lines represent bedding in the periclinal area of some fold-related thrust. c) Normal limb in ORD1 and regional cleavage. d)Nummulite Marls. SA1: normal/long limb, SA2: overturned/short limb. d1) SA fold with location of both sites. d2) Regional cleavage (dashed line) and bedding plane (continuous line) shown in the normal limb. Steroplots with geographic projection where bedding and cleavage are represented, legend as in Fig. 2.

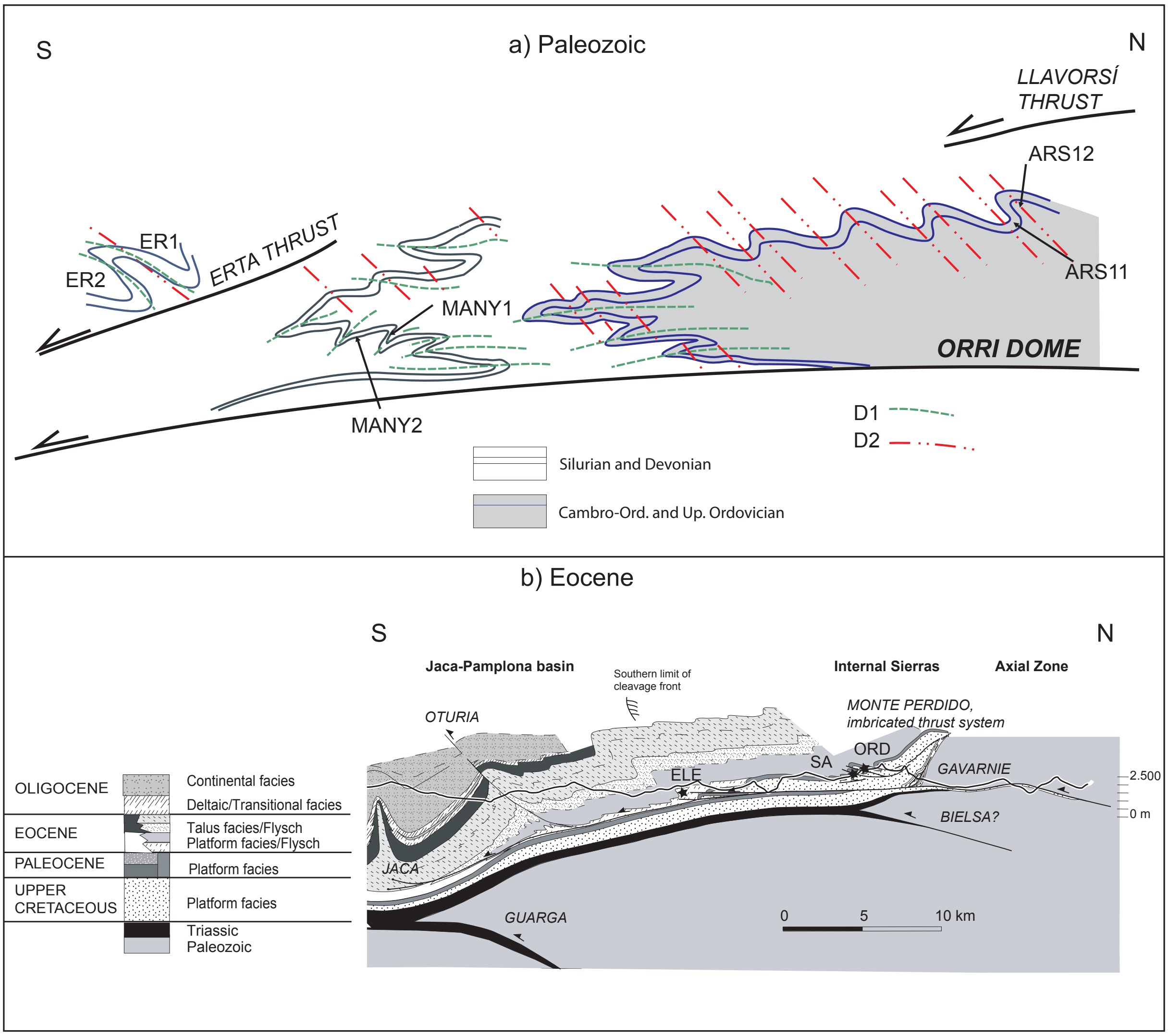

Fig. 4. a) Simplified cross-section of the two phases of deformation and S_1/S_2 associated cleavage affecting Paleozoic rocks. b) Cross-section showing the structural position of three folds affecting Eocene rocks (modified from Oliva-Urcia, 2004).

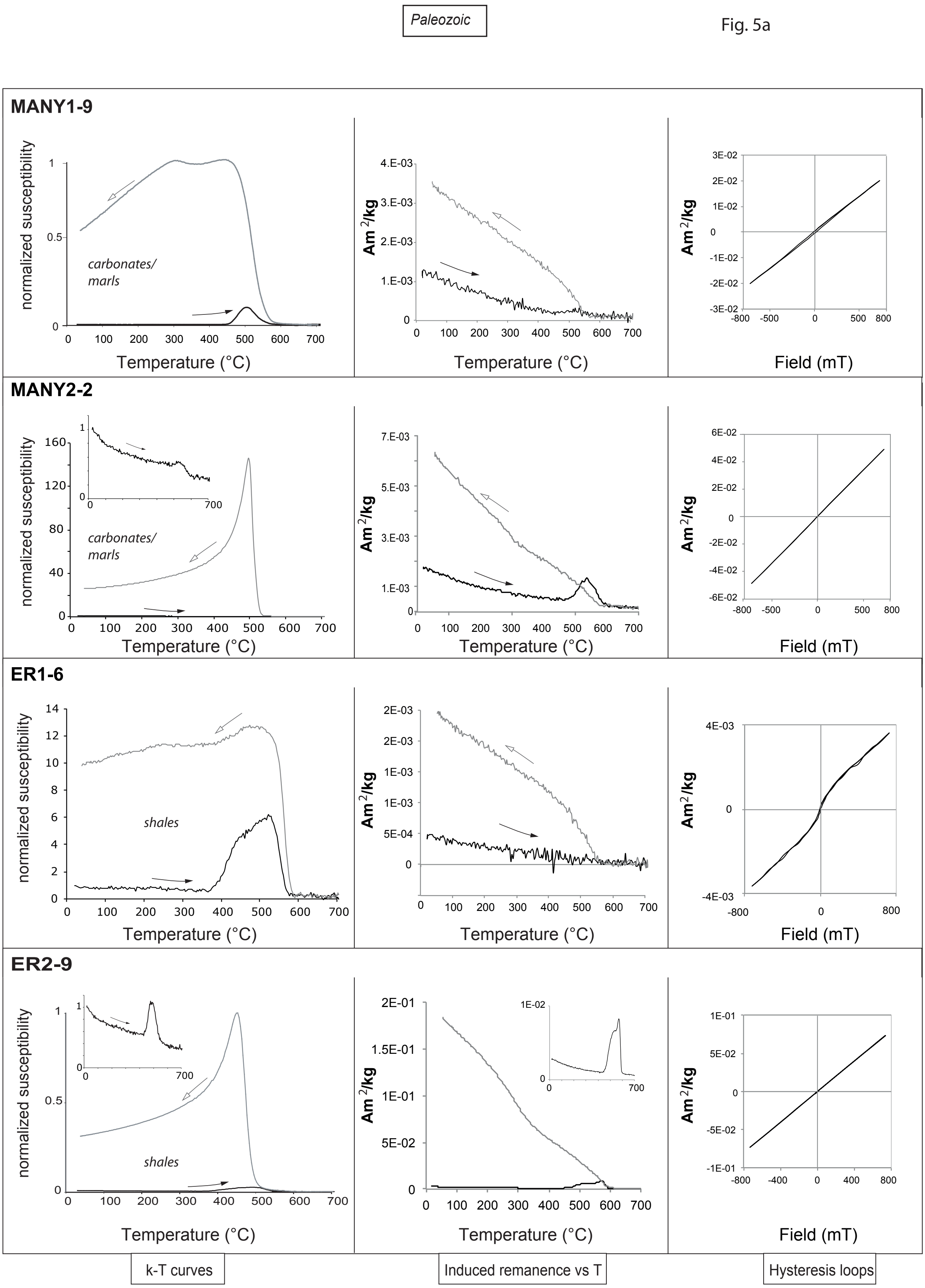

Fig. 5. Temperature dependence of magnetic susceptibility curves, remanent magentization M_r acquired after application of 268 Oe, and induced magentization M as function of applied field (hysteresis loops) for selected Paleozoic samples.

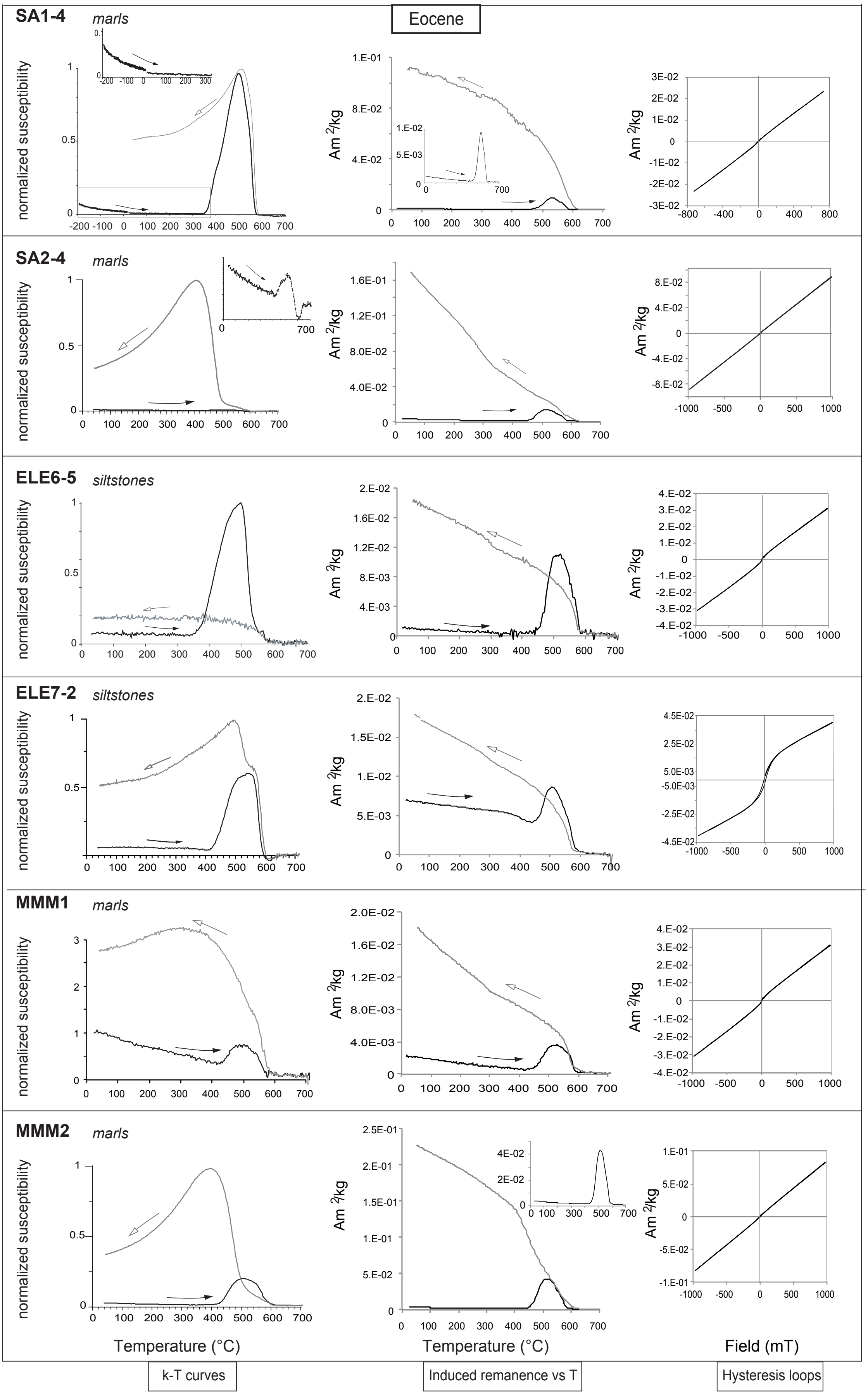

Fig. 6. The same as in Fig. 5, but for selected Eocene samples.

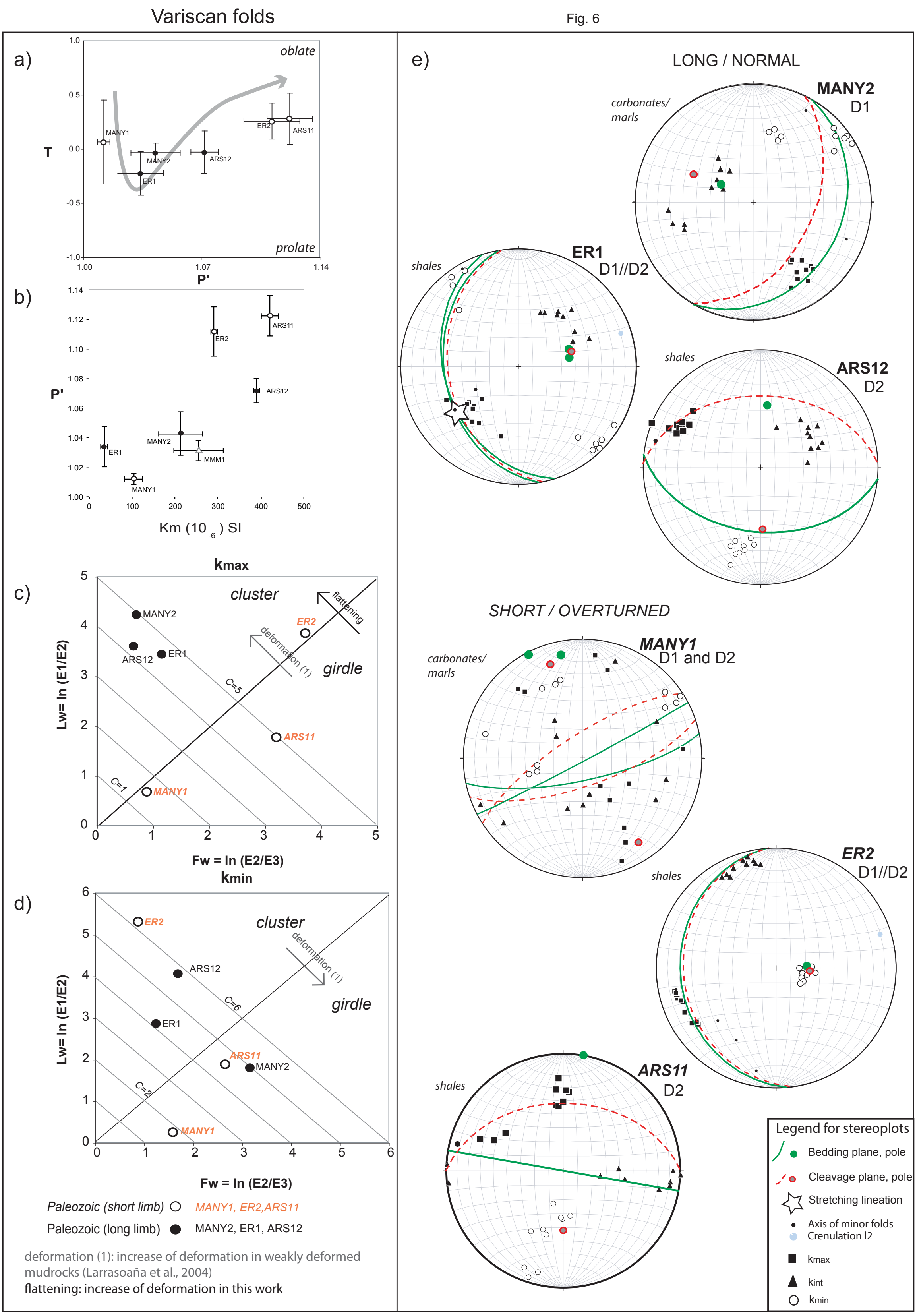

Fig. 7. a) Average values of magnetic susceptibility of the Paleozoic rocks for every site, shape parameter (T) and corrected anisotropy degree (P'); b) P' and bulk susceptibility (κ_{mean}) diagram; c) Woodcock diagram for k_{max} axes and d) Woodcock diagram for κ_{min} axes (see text for more detail); increase of deformation is marked with a grey arrow for weakly deformed rocks (Larrasoaña et al., 2004); e) stereographic projections in geographical coordinates of the magnetic ellipsoid axes.

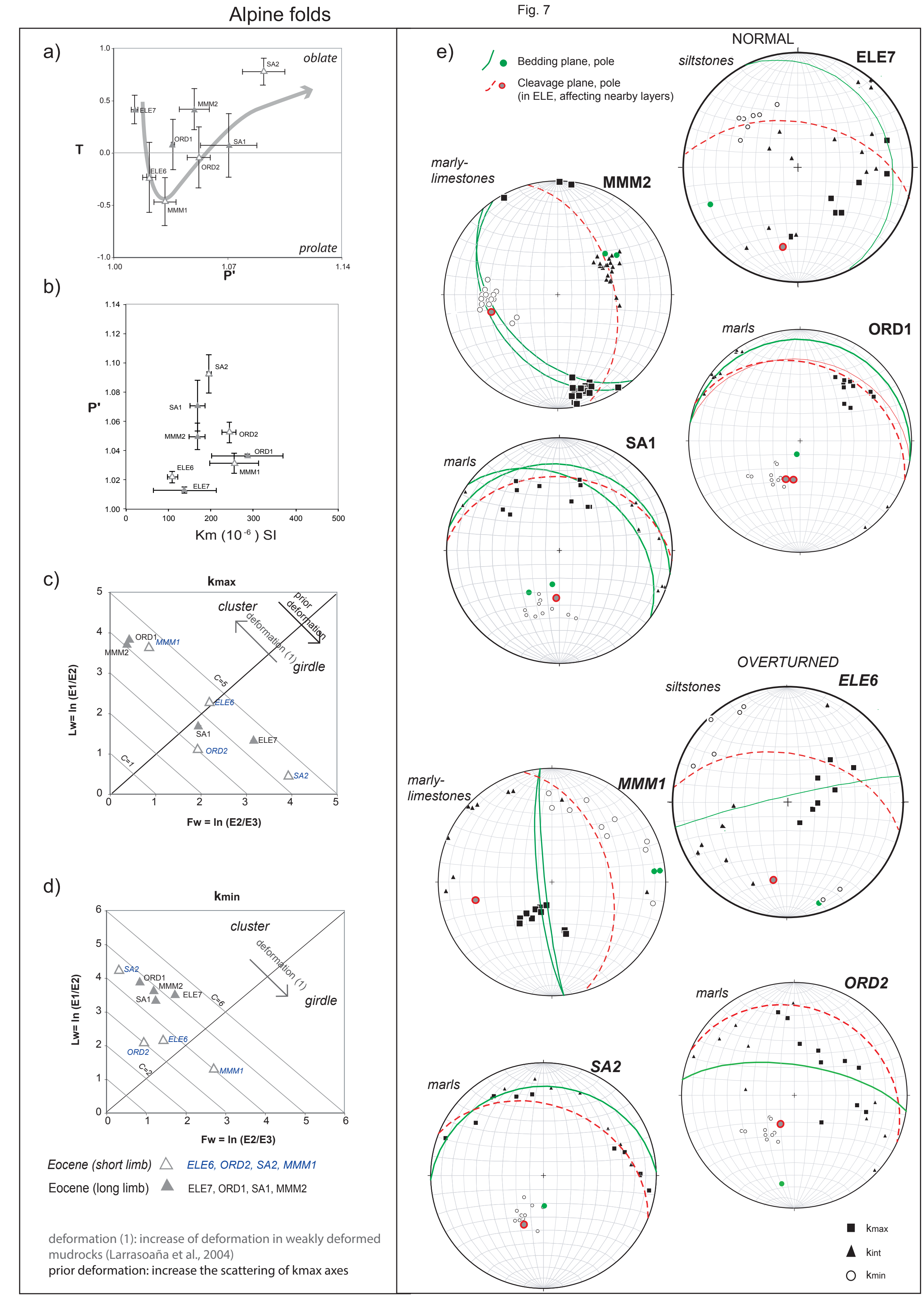

891
892 Fig. 8. The same as in Fig. 7, but for the Eocene rocks.

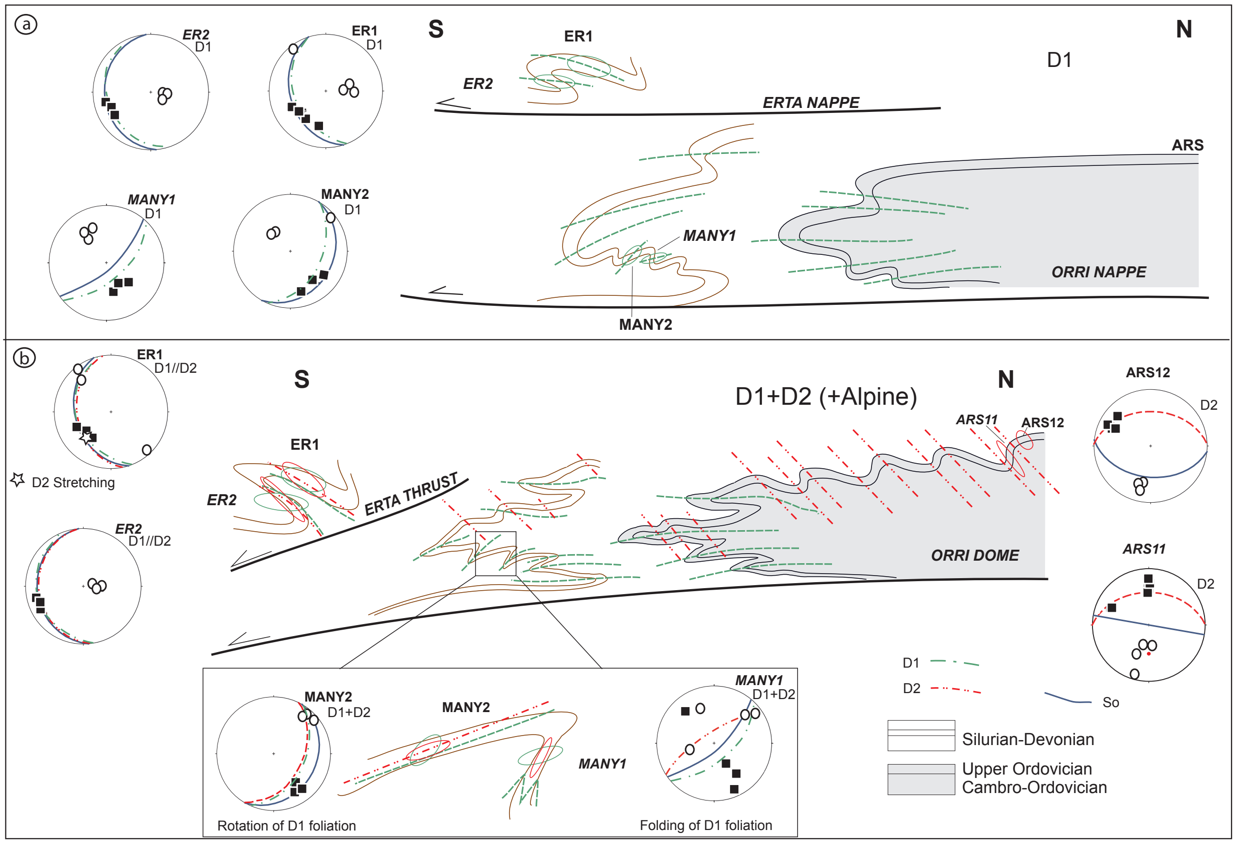

Fig. 9. a) General model for the development of the magnetic fabric in Paleozoic rocks f or de D1 deformational phase, and b) the final situation of the petrofabric in the D2 deformational phase.

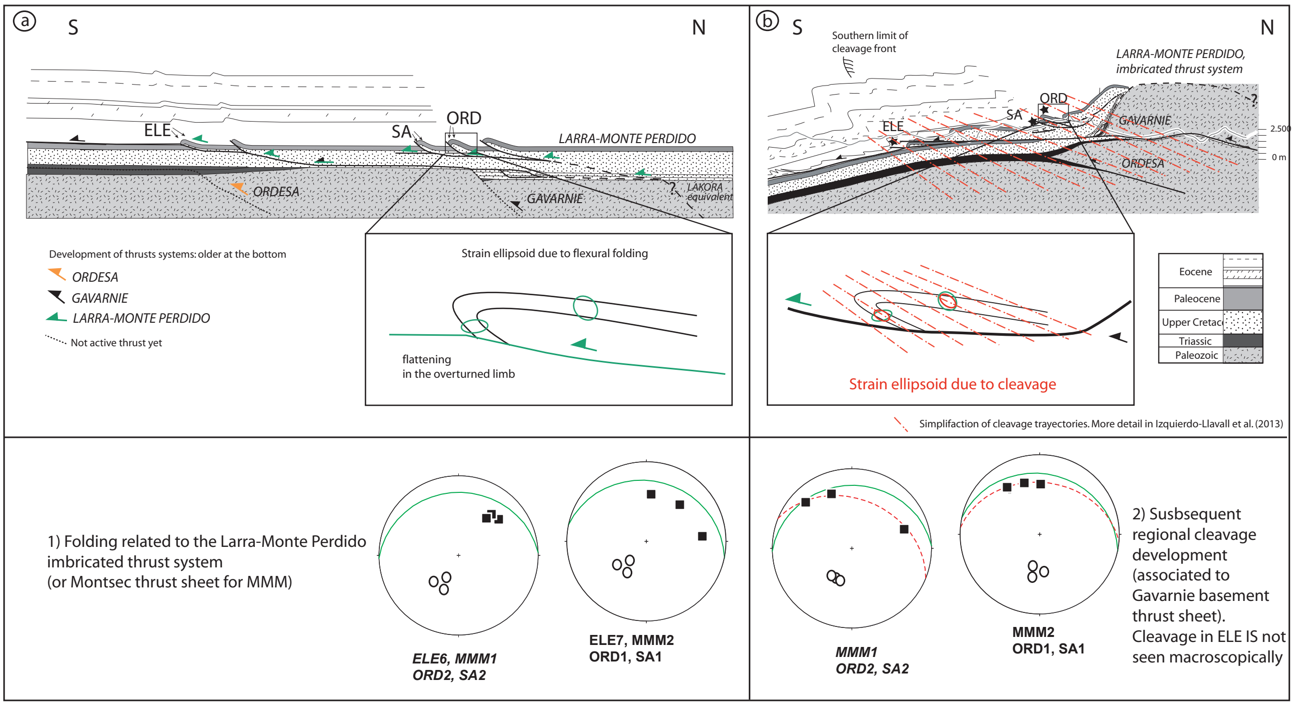

Fig. 10. Evolution of the magnetic fabric in the folds developed in Eocene rocks. a) Folding due to the Larra-Monte Perdido thrust system, and b) superposition of the cleavage development due to the activity of the basement thrust sheets (mainly Gavarnie). Simplified cross sections based on Oliva-Urcia (2004).